



This open access document is published as a preprint in the Beilstein Archives with doi: 10.3762/bxiv.2020.1.v1 and is considered to be an early communication for feedback before peer review. Before citing this document, please check if a final, peer-reviewed version has been published in the Beilstein Journal of Nanotechnology.

This document is not formatted, has not undergone copyediting or typesetting, and may contain errors, unsubstantiated scientific claims or preliminary data.

Preprint Title Preparation, characterization and photocatalytic performance of hetero-structured CuO-ZnO loaded composite nanofiber membranes

Authors Wei Fang, Liang Yu and Lan Xu

Publication Date 02 Jan 2020

Article Type Full Research Paper

ORCID® iDs Lan Xu - <https://orcid.org/0000-0003-2185-4104>

Preparation, characterization and photocatalytic performance of hetero-structured CuO-ZnO loaded composite nanofiber membranes

Wei Fang[†], Liang Yu[†] and Lan Xu*

National Engineering Laboratory for Modern Silk, College of Textile and Engineering, Soochow University, 199 Ren-ai Road, Suzhou 215123, China

*Correspondence: lanxu@suda.edu.cn; Tel.: +86-512-65884521 (L.X.)

[†] W. Fang and L. Yu contributed equally to this paper

ABSTRACT

Owing to the nano-effect of nanofibers and special properties of semiconductor oxides, inorganic semiconductor oxides loaded composite nanofibers (CNFs) have been widely applied in environmental monitoring, industry, aviation, transportation and other fields. In this paper, the hetero-structured CuO-ZnO loaded CNF membranes (CNFMs) were prepared successfully by a combination of electrospinning technology, heat treatment and hydrothermal method. The effects of electrospinning, heat treatment and hydrothermal parameters on morphology, structure and properties of the CNFMs were investigated, and the optimal process parameters were determined. Then the hetero-structured CuO-ZnO loaded CNFMs obtained under the condition of the optimal process parameters were applied to photocatalytic degradation of methyl orange, and it was found the CNFMs could be reused to degrade methyl orange at least three times, and the degradation rate remained above 90%.

Keywords: electrospinning; semiconductor oxide; composite nanofibers; hetero-structured CuO-ZnO; hydrothermal; photocatalytic

1. Introduction

Water remediation is one of the main scientific research subjects of environmental protection. And water pollution with organic dyes (such as congo red, methylene blue, methyl orange etc.) is becoming a major environmental problem through the world. Therefore, water purification technologies, such as photocatalytic purification, electrochemical oxidation, membrane filtration, ozonation, chlorination flocculation and et al., have attracted much attention recently [1-3]. Photocatalytic purification of water has the advantages of high efficiency, thoroughness and no secondary pollution, and can thoroughly oxidize various refractory organic pollutants in the water to non-toxic and harmless substances. It will become the main means of terminal treatment of water and air pollutants [4].

Photocatalytic reactions on the metal oxide semiconductors are of many interests due to their capability to the treatment of a lots of pollutants [5]. The photoinduced electrons and holes can reduce and oxidize species adsorbed on the semiconductors because of the band gap excitation, however, there is a disadvantage, which is the high degree of recombination between the photogenerated charge carriers [6]. Many studies have been focused on the mixed metal oxide semiconductors due to an efficient charge separation obtained by coupling two different semiconductors, which result in a vectorial transfer of photogenerated electrons and holes from a semiconductor to another [7-10].

ZnO has been widely applied as a semiconductor due to its wide direct band gap (3.2 eV) which absorbs a small portion of solar spectrum in the UV region[11-13]. CuO is a nontoxic, chemically stable and naturally abundant material as a p-type semiconductor with a reported direct band gap of 1.2-1.79 eV [14]. Because of its narrow band gap, CuO is usually used in combination with large band gap semiconductor, such as ZnO and TiO₂, to improve their photocatalytic activity under solar light irradiation [15]. It was reported that the p-n heterojunction composed of ZnO and CuO had a selective photocatalytic activity because the formation of p-n heterojunction could cause a better charge separation [16-22]. Liu et al. [23] prepared CuO/ZnO nanocomposites by homogeneous coprecipitation method of coordination oxidation and used it for photocatalytic degradation of methyl orange. Wei et al. [24] fabricated CuO/ZnO composite nanofilms using cathodic co-electrodeposition and observed its photocatalytic performance. Fierro et al. [25] synthesized CuO-ZnO composite catalysts by temperature-programmed reduction and applied them to photocatalytic degradation.

Nanocomposites loaded with metal oxide semiconductors have excellent optical, electrical, mechanical and chemical properties, which result in their great potential applications in photocatalysis[26]. Electrospinning provides a simple and convenient method for generating composite nanofibers (CNFs) [27-31]. There are many outstanding characteristics of CNFs, such as high ratio of surface area, superior thermal and mechanical properties, which could be widely used as a carrier[32, 33]. In recent years, CNFs loaded with metal oxide nanoparticles have attracted a great deal of attention in the photocatalytic purification of water. He et al. [34] fabricated porous Graphene/TiO₂ CNFs by electrospinning and observed their photocatalytic performance. Yuan et al. [35] obtained TiO₂/WO₃ CNFs using electrospinning and applied them to photocatalytic of mercury removal. Teng et al. [36] prepared TiO₂/NiO CNFs by electrospinning and used them for photocatalysis.

In the present study, the hetero-structured CuO-ZnO loaded CNF membranes (CNFMs) were prepared using a combination of electrospinning technology, heat treatment and hydrothermal method. The effects of electrospinning, heat treatment and hydrothermal parameters on morphology, structure and properties of the CNFMs were investigated, and the optimal process parameters were determined. The CuO-ZnO heterojunction was successfully grown on the surface of PVDF/PAN CNFMs, and was applied to photocatalytic degradation of methyl orange, which could be well exploited as an efficient adsorbent for removal of methyl orange dye.

2. Experiment

2.1 Materials

Anhydrous copper acetate (Cu(Ac)₂, Mw=181.63) and anhydrous zinc acetate (Zn(Ac)₂, Mw=183.48) were supplied by Shanghai Macklin Biochemical Co., Ltd. and Aladdin industrial Corporation (shanghai, china), respectively. Polyacrylonitrile (PAN, Mw=150,000) powders were purchased from Beijing Lark Branch Co., Ltd. (Beijing, China). Polyvinylidene fluoride (PVDF, Mw=400,000) and N,N-dimethylformamide (DMF) were provided from Shanghai Chemical Reagent Co., Ltd. (Shanghai, China). Anhydrous copper sulfate (CuSO₄, Mw=159.60), zinc chloride (ZnCl₂, Mw=73.09), hexamethylenetetramine (C₆H₁₂N₄, Mw=140.19) and ammonia (NH₃•H₂O, Mw=17.03) were supplied from China Pharmaceutical Group Chemical Reagents Co., Ltd. (Shanghai, China). Methyl orange (Mw = 327.34) was purchased from Shanghai Debai Biotechnology Co., Ltd. (Shanghai, China). All materials were of analytical grade and

applied without any further purification.

2.2 Preparation of hetero-structured CuO-ZnO loaded CNFMs

The hetero-structured CuO-ZnO loaded CNFMs were prepared by a combination of electrospinning, heat treatment and hydrothermal method, as shown in Fig.1.

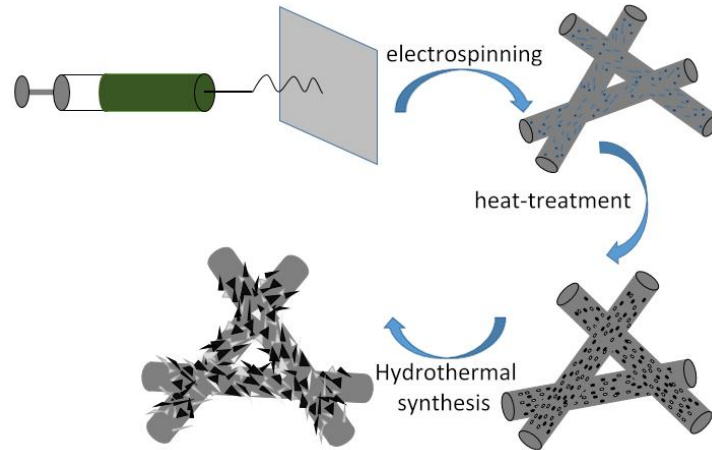


Figure 1. Schematic of preparation of the hetero-structured CuO-ZnO loaded CNFMs.

2.2.1 Electrospinning process

Preparation of spinning solution

The mixed solutions of PVDF and PAN were prepared with 8 wt% by dissolving a mixture of PVDF and PAN with different weight ratios (9:1, 7:3, 5:5, 3:7 and 1:9) into DMF. The obtained solutions were magnetically stirred for 2h at 80°C until they became homogeneous. Then, the same amounts of $\text{Cu}(\text{Ac})_2$ and $\text{Zn}(\text{Ac})_2$ were added into the mixed solutions of PVDF and PAN, and were dispersed in the solutions by an ultrasonic cleaner (SL-5200DT, Nanjing Shunliu Instrument Co.Ltd., China) for 2h at room temperature ($25\pm 2^\circ\text{C}$). The weight ratios of the added total amounts of $\text{Cu}(\text{Ac})_2$ and $\text{Zn}(\text{Ac})_2$ to the mixture of PVDF and PAN were respectively 1:5, 1:3 and 1:2.

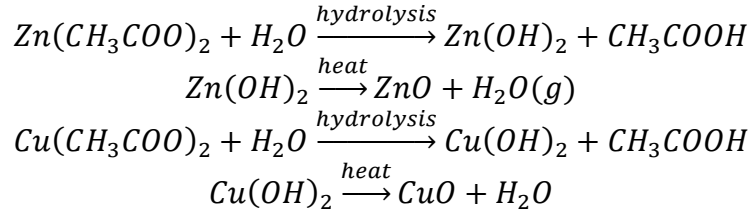
Preparation of electrospun $\text{Cu}(\text{Ac})_2/\text{Zn}(\text{Ac})_2/\text{PVDF}/\text{PAN}$ CNFMs

The prepared spinning solution was taken in the 10ml syringe and delivered with a flow rate of 0.6ml/h by a syringe pump. The applied voltage and the distance from needle tip to collector were respectively maintained at 20kv and 18cm. The electrospinning experiments were carried out at room temperature ($25\pm 2^\circ\text{C}$) and a relative humidity of ($55\pm 5\%$), and the electrospun $\text{Cu}(\text{Ac})_2/\text{Zn}(\text{Ac})_2/\text{PVDF}/\text{PAN}$ CNFMs were collected and carefully peeled off from the aluminium foil.

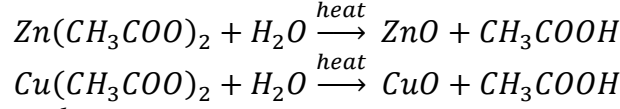
2.2.2 Heat treatment process

The collected $\text{Cu}(\text{Ac})_2/\text{Zn}(\text{Ac})_2/\text{PVDF}/\text{PAN}$ CNFMs were cut into several pieces with a square area of $3\text{cm}\times 3\text{cm}$, and put into the Muffle furnace (GZ2.5-10TP, Shanghai Gaozhi Precision Instrument Co., Ltd., China) where it would be calcined for a period of time. The heating rate was kept at $5^\circ\text{C}/\text{min}$ in the heat treatment process. The heat treatment temperatures varied from 80 to 180°C .

A simple chemical solution strategy was used to form $\text{Cu}(\text{OH})_2$ and $\text{Zn}(\text{OH})_2$, and then CuO and ZnO nanoparticles were successfully obtained by the heat treatment process, as shown in the following equations[16].



or



2.2.3 Hydrothermal process

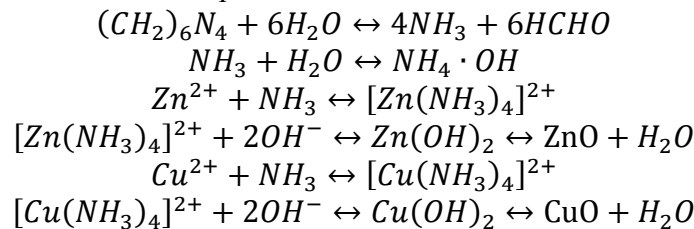
Preparation of growth solution

The growth solutions, used in the hydrothermal process, were obtained by preparing mixtures of $\text{C}_6\text{H}_{12}\text{N}_4$, $\text{NH}_3 \cdot \text{H}_2\text{O}$ and saturated aqueous solution of CuSO_4 and ZnCl_2 . The saturated aqueous solution of CuSO_4 and ZnCl_2 was prepared by dissolving excessive CuSO_4 and ZnCl_2 into 100 ml deionized water. Next the saturated aqueous solutions of CuSO_4 and ZnCl_2 were diluted, and three different concentrations of CuSO_4 and ZnCl_2 aqueous solutions with dilution of 1, 5 and 25 times were obtained respectively. Then excessive $\text{C}_6\text{H}_{12}\text{N}_4$ powders were added respectively into the solutions with four different concentration gradients and were stirred sufficiently. Subsequently, $\text{NH}_3 \cdot \text{H}_2\text{O}$ was dripped into the above solutions and stirred fully until the solutions became clarified. Finally, 3-5 drops of $\text{NH}_3 \cdot \text{H}_2\text{O}$ were added into the four solutions respectively, and the four prepared growth solutions were sealed for the following hydrothermal process.

Preparation of hetero-structured CuO-ZnO loaded CNFMs

The calcined CNFMs were fixed on glass sheets and put in four 50ml reaction kettles which contained 10ml of the above four growth solutions obtained, respectively. After tightening the cover of the reaction kettle, it was placed in an electrothermal oven with adjusting heat temperature and time (DHG-9030A, Shanghai Shenxian Constant Temperature Equipment Factory, China). At the end of the set reaction time, the fabricated hetero-structured CuO-ZnO loaded CNFMs were taken out with tweezers, and were rinsed repeatedly with deionized water for several times. Next, the rinsed CNFMs were dried in the electrothermal oven, and then the dried CNFMs were packed in self-sealing bags for subsequent tests and applications.

The mechanism of growth of CuO and ZnO nanocrystals on the calcined CNFMs by hydrothermal method could be explained as follows:



For comparison, CuO loaded PVDF/PAN CNFMs and ZnO loaded PVDF/PAN CNFMs were also prepared by the same method, respectively.

2.3 Measurement and characterization

Diameter and arrangement of CNFMs were investigated by a scanning electron

microscopy (SEM, Hitachi S-4800, Japan). The matrix morphology and fibrous diameter distribution were carried out using Image J software (National Institute of Mental Health, Bethesda, Maryland, USA). And 100 fibrous diameter at random in each sample were chosen for diameter characterization. In addition, an energy dispersion spectroscopy (EDS, Hitachi S-4800, Japan) was used to identify the elemental composition of a sample region evaluated with SEM analysis. During EDS, the sample was exposed to an electron beam inside SEM, and the elemental composition of the sample could be determined by analyzing the emitted x-rays.

The pore size distributions of CNFMs were measured using a capillary flow porometry (Porometer 3G, Quantachrome Instruments, USA). All samples were circular membranes with the diameter of 25 mm and the thickness of 10 μm .

FTIR spectra of CNFMs were obtained using a Fourier transform infrared (FTIR) spectroscopy (Nicolet5700, Thermo Nicolet Company, Waltham, MA, USA) by the performance of 32 scans within the wavenumber range of 400-4000 cm^{-1} with a resolution of 4 cm^{-1} . X-ray diffraction (XRD) analyses were used to illustrate the crystalline structures of CNFMs using Philips X'Pert-Pro MPD (PANalytical, Almelo & Eindhoven, The Netherlands).

The mechanical properties of CNFMs were characterized using a universal electromechanical test machine Instron-3365 (Instron, Norwood, MA, USA). All samples were 4cm \times 1cm rectangle membranes, and the measurement of each sample was repeated five times.

Contact angle (CA) measurements of CNFMs were carried out by a Krüss K100 apparatus (Krüss Company, Hamburg, Germany). The deionized water droplet of 6 μL was used for static CA measurements, and the average CAs were determined by measuring five different positions of the same sample.

2.4 Photocatalytic degradation process

Photocatalytic degradation processes under ultraviolet (UV) irradiation were investigated using the prepared CNFMs degrading methyl orange solution with an initial concentration of 10 mg/L. The prepared CNFMs of 0.05 g were put into the methyl orange solution of 30 ml, and then the solution was placed in dark environment for 2 hours to achieve adsorption-desorption equilibrium. Next, the experiments of photocatalytic degradation of methyl orange were carried out under an UV lamp (20W, 254nm). Degradation rate of methyl orange solutions at different time intervals was determined by measuring the variation in maximum absorbance of methyl orange at 465 nm using UV spectrophotometer (Cary 5000, Agilent Technologies, USA).

3. Results and discussion

3.1 Characterization of electrospun Cu(Ac)₂/Zn(Ac)₂/PVDF/PAN CNFMs

Cu(Ac)₂/Zn(Ac)₂/PVDF/PAN CNFMs were fabricated using electrospinning, and the effects of different component contents on morphology, structure and properties of the CNFMs were investigated by a combination of SEM, FTIR, XRD, and et al.

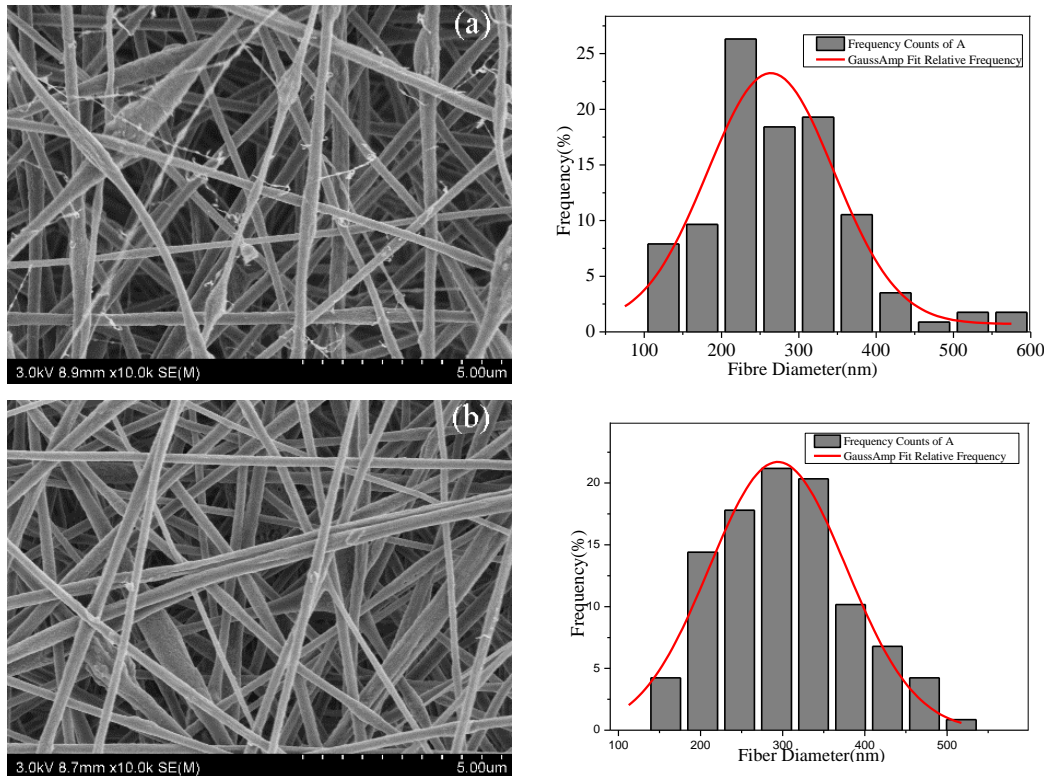
3.1.1 Effect of the weight ratio of PVDF to PAN on the electrospun CNFMs

The electrospun Cu(Ac)₂/Zn(Ac)₂/PVDF/PAN CNFMs with the weight ratio (Cu(Ac)₂/Zn(Ac)₂:PVDF/PAN=1:3) were prepared, and the effects of the weight ratio of PVDF to PAN on the CNFMs were indicated.

Morphological characterization (SEM)

The morphologies of the CNFMs with different weight ratios of PVDF to PAN were characterized by SEM. The SEM images of the electrospun CNFMs and the according nanofiber diameter distributions were presented in Fig.2. And the effect of the weight ratio (PVDF: PAN) on the nanofiber diameters of the CNFMs was illustrated in Table 1. It could be seen that the average nanofiber diameters of the CNFMs were all in the range of 200-300 nm, and with the decrease of the weight ratio (PVDF: PAN) the average nanofiber diameters of the CNFMs decreased due to decreased average molecular weight [37]. But when the weight ratio was 1:9 the average nanofiber diameter increased slightly due to the appearance of beads, as exhibited in Fig.2 (e).

In addition, Fig.2 showed when the weight ratio (PVDF: PAN) was 9:1 the nanofiber diameter distributions of the CNFMs were non-uniform, and some filaments and beads were entangled in them. As the weight ratio decreased, the number of filaments and beads decreased significantly. When it reached 5:5, the nanofiber diameter distributions of the CNFMs were uniform, and there were no filaments and beads. With further decreased the weight ratio, there appeared filaments and beads in the CNFMs, resulting in the uneven distribution of nanofiber diameter. Therefore, the weight ratio of 5:5 was selected as the optimal parameter in the following experiments.



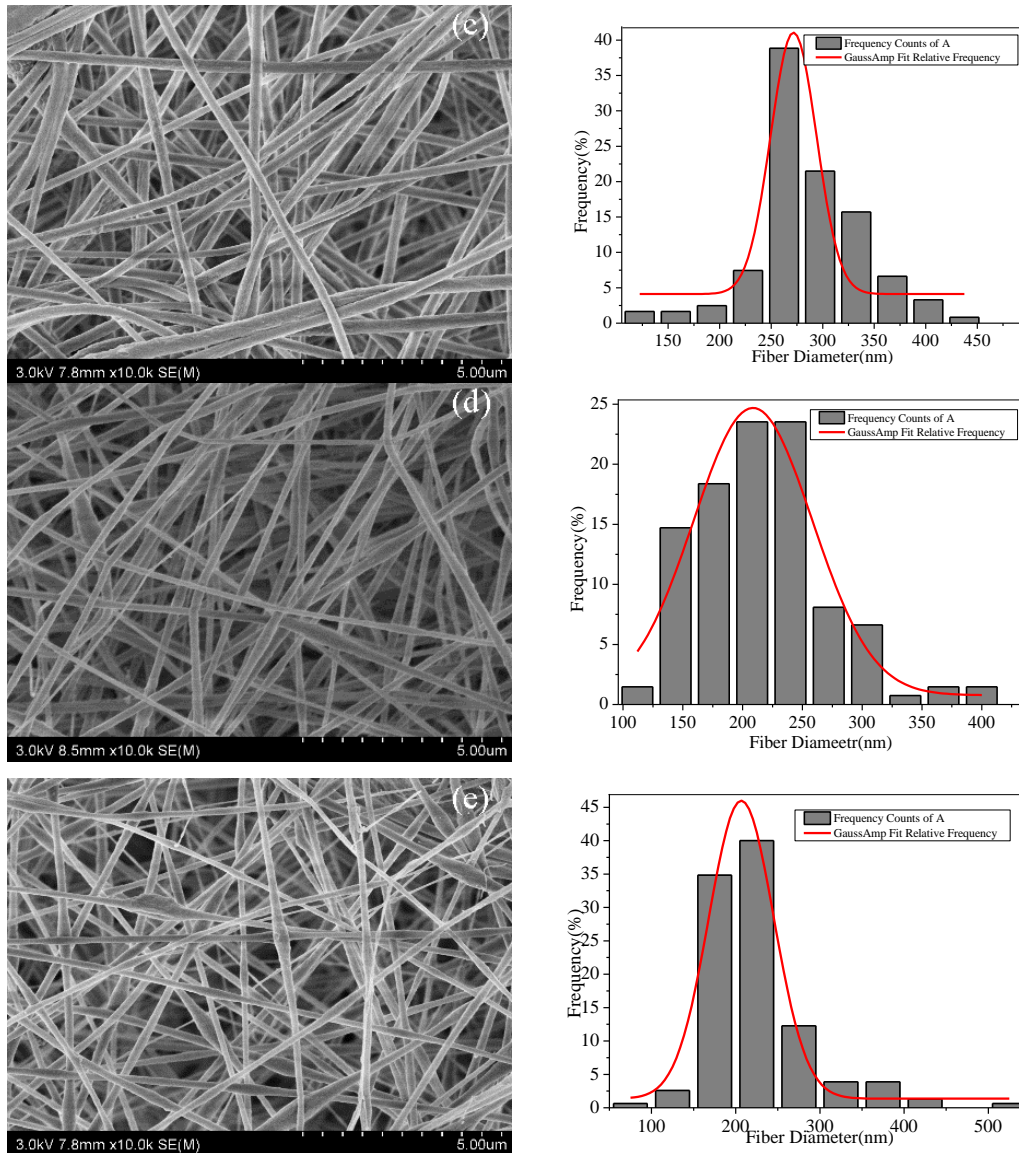


Figure 2. SEM images of the electrospun CNFMs with different weight ratios of PVDF to PAN ((a) 9:1; (b) 7:3; (c) 5:5; (d) 3:7; (e) 1:9). The right figures were the according nanofiber diameter distributions.

Table 1. Average nanofiber diameters of the electrospun CNFMs with different weight ratios (PVDF: PAN).

PVDF: PAN	Average diameter (nm)	Standard deviation (nm)	Confidence interval (nm)
9:1	275	94.0	±18.4
7:3	302	80.8	±15.8
5:5	284	51.5	±10.1
3:7	216	82.0	±16.1
1:9	227	60.1	±12.0

Pore size distribution of the electrospun CNFMs

The pore size distributions of the CNFMs with different weight ratios (PVDF: PAN) determined by a capillary flow porometry were illustrated in Fig.3, and the measured data of pore sizes were exhibited in Table 2. It was obvious that when the weight ratio 3:7 the

pore sizes of the CNFMs were the smallest, and when the weight ratio 7:3 the pore sizes of the CNFMs were the largest. Compared with the nanofiber diameters of the CNFMs presented in Table 1, it can be found that the pore sizes of the CNFMs were mainly determined by the nanofiber diameters of that. The larger the nanofiber diameters were, the larger the pore sizes would be.

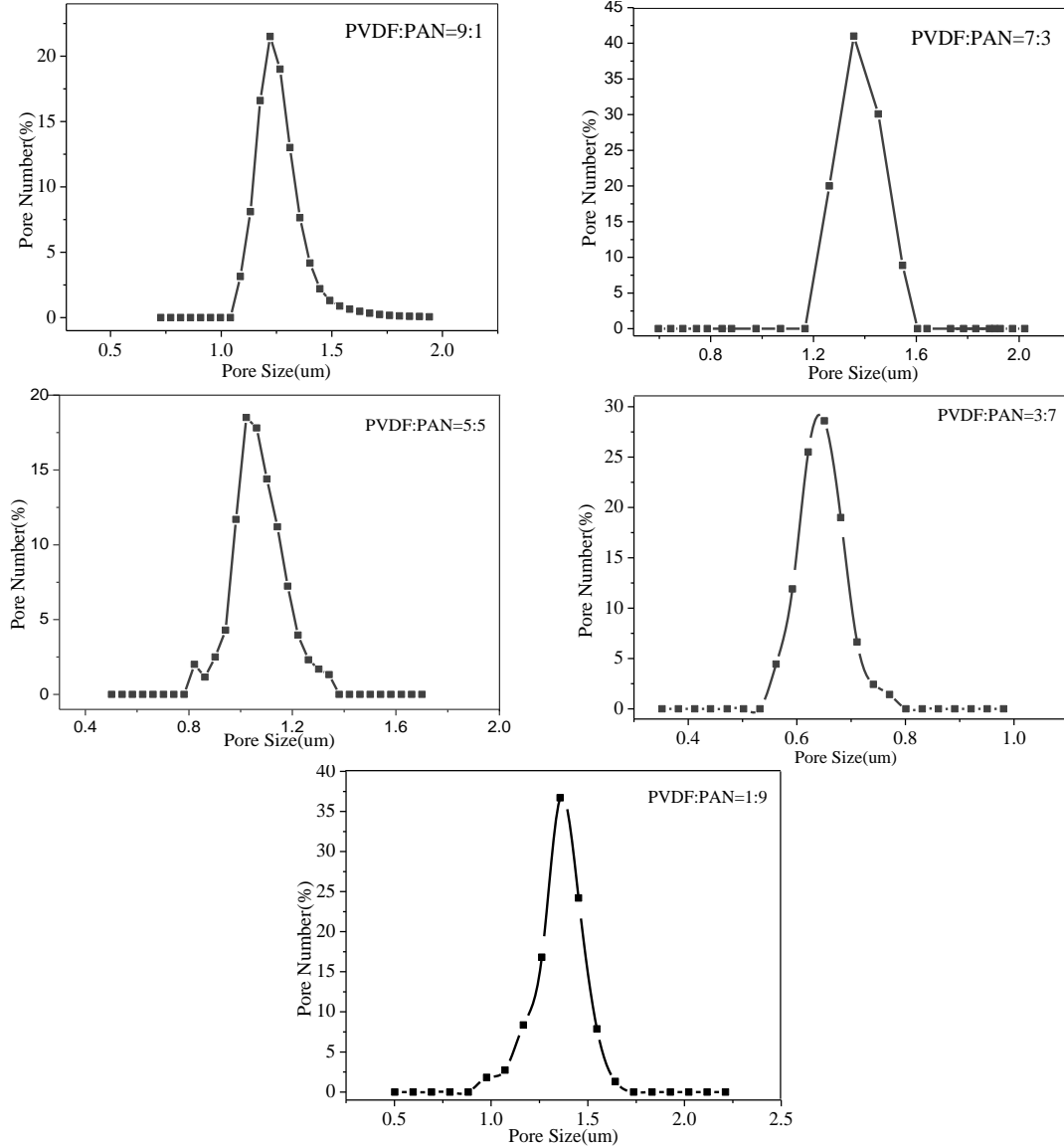


Figure 3. The pore size distributions of the CNFMs with different weight ratios (PVDF: PAN).

Table 2. The measured data of pore size distributions of the CNFMs with different weight ratios (PVDF: PAN).

PEG: PLA	Pore size (μm)	Pore size corresponding to the maximum pore number (μm)
9:1	1.087-1.781	1.363
7:3	1.262-1.642	1.452
5:5	0.822-1.342	1.062
3:7	0.562-0.771	0.681

Wetting property

The CA values of the CNFMs with different weight ratios (PVDF: PAN) measured were displayed in Figure 4. It could be seen that all the CNFMs were hydrophobic, and the hydrophobicity of the CNFMs reduced slightly as the weight ratio decreased. The reason might be that the hydrophobicity of pure PVDF nanofiber membranes (NFMs) was stronger than that of pure PAN NFMs. And nanofiber diameter distribution, thickness and surface roughening of the CNFMs could lead to the difference in the hydrophobicity.

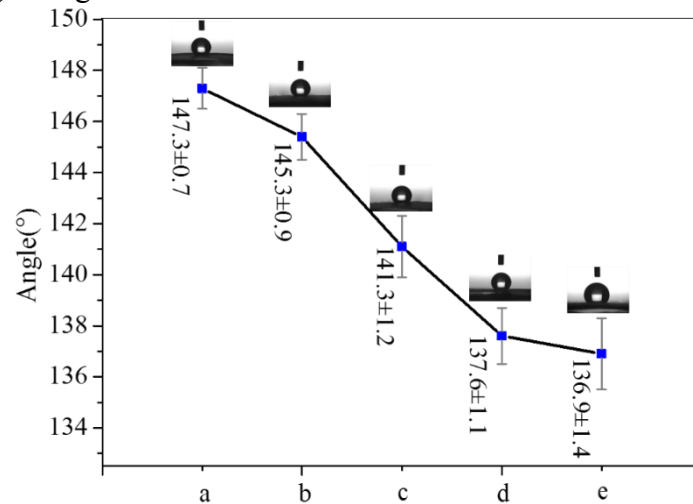


Figure 4. Contact angles of the CNFMs with different weight ratios (PVDF: PAN) ((a) 9:1; (b) 7:3; (c) 5:5; (d) 3:7; (e) 1:9).

Mechanical property

The mechanical properties of the CNFMs with different weight ratios (PVDF: PAN) were exhibited in Fig.5. It could be find that with the decrease of the weight ratio the breaking elongation of the CNFMs decreased gradually and the tensile strength of that increased slowly, resulting in better strength and poor flexibility of the CNFMs. Therefore, the CNFMs with relatively good mechanical properties could be obtained by blending PVDF and PAN in a certain weight ratio.

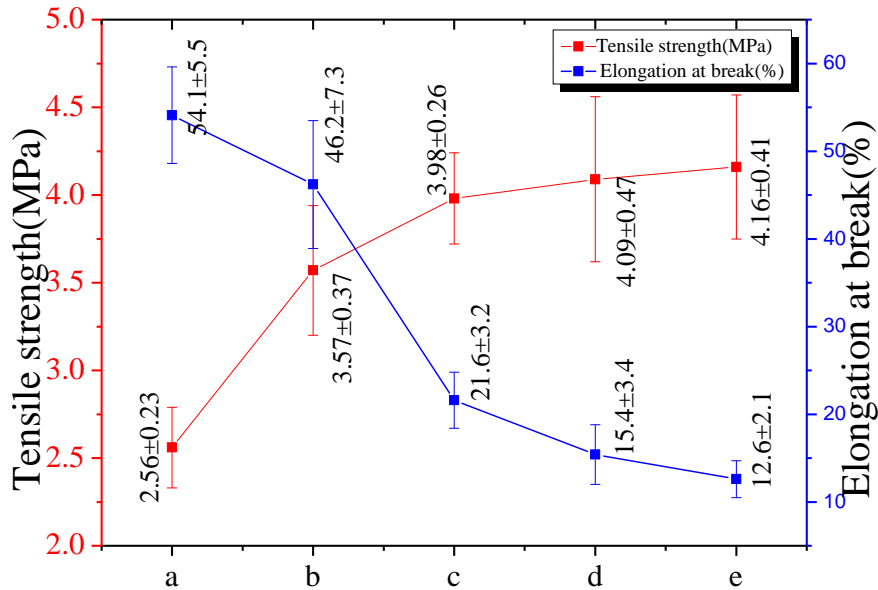


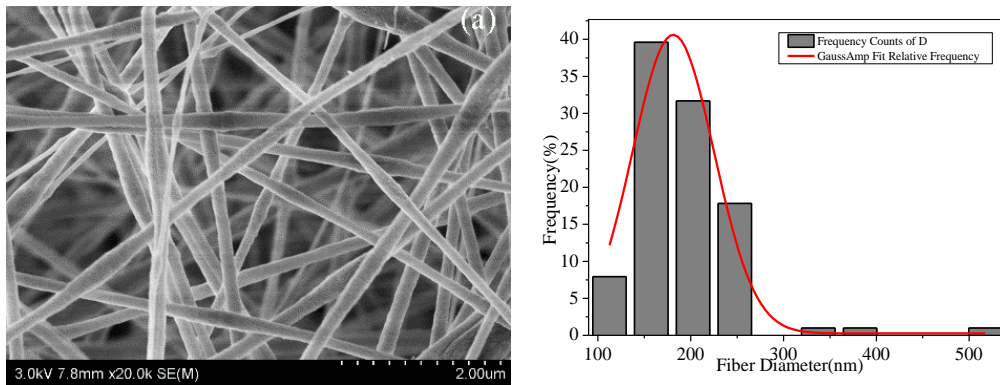
Figure 5. Mechanical properties of the CNFMs with different weight ratios (PVDF: PAN) ((a) 9:1; (b) 7:3; (c) 5:5; (d) 3:7; (e) 1:9).

3.1.2 Effect of the additive content of $Cu(Ac)_2$ and $Zn(Ac)_2$ on the CNFMs

The electrospun $Cu(Ac)_2/n(Ac)_2/PVDF/PAN$ CNFMs with the weight ratio (PVDF: PAN = 5:5) were fabricated, and the effects of the weight ratio of $Cu(Ac)_2$ and $Zn(Ac)_2$ to PAN and PVDF on the CNFMs were illustrated.

Morphological characterization (SEM)

The SEM images of the CNFMs with the different weight ratios of $Cu(Ac)_2$ and $Zn(Ac)_2$ to PAN and PVDF were presented in Figure 6, including the according nanofiber diameter distributions. And the effect of the weight ratio ($Cu(Ac)_2/Zn(Ac)_2$: PVDF/PAN) on the nanofiber diameters of the CNFMs was illustrated in Table 3.



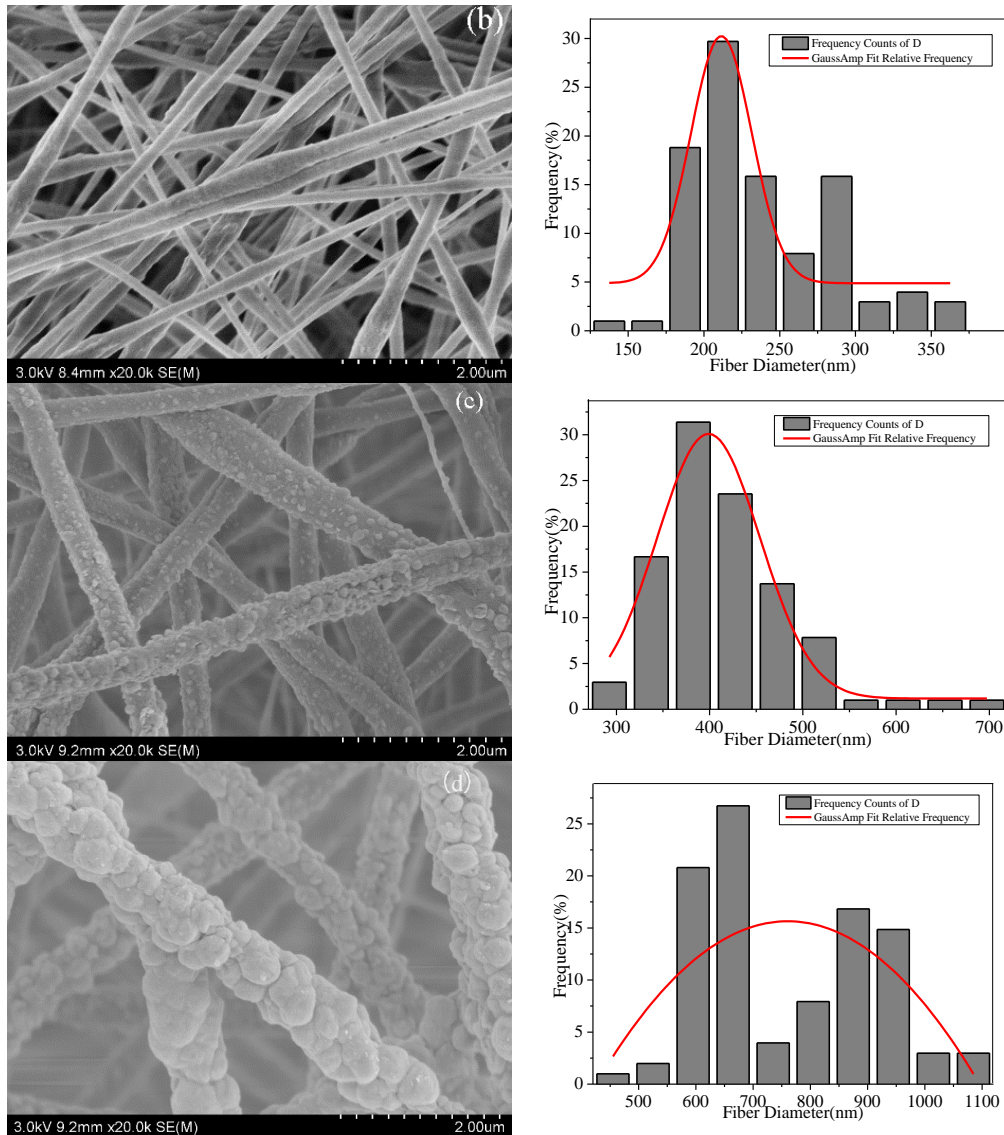


Figure 6. SEM images of the electrospun CNFMs with different weight ratios of Cu(Ac)₂ and Zn(Ac)₂ to PAN and PVDF ((a)1:5; (b)1:3; (c)1:2; (d)1:1). The right figures were the according nanofiber diameter distributions.

Table 3. Average nanofiber diameters of the electrospun CNFMs with different weight ratios (Cu(Ac)₂/Zn(Ac)₂: PVDF/PAN).

Cu(Ac) ₂ /Zn(Ac) ₂ : PVDF/PAN	Average diameter (nm)	Standard deviation (nm)	Confidence interval (nm)
1:5	193	52.7	±10.3
1:3	236	47.9	±9.4
1:2	414	70.8	±13.9
1:1	758	148.5	±29.1

As could be seen from Fig.6 and Table 3, as the weight ratio (Cu(Ac)₂/Zn(Ac)₂: PVDF/PAN) increased, the average nanofiber diameters of the CNFMs increased and their surface changed from smooth to rough. This was because when the additive contents of Cu(Ac)₂ and Zn(Ac)₂ particles was less, they were wrapped fully inside the nanofibers.

But with the increase of the particles, there appeared gradually particles on the surface of the nanofibers. When the weight ratio ($\text{Cu}(\text{Ac})_2/\text{Zn}(\text{Ac})_2$: PVDF/PAN) was 1:5 or 1:3, there appeared fewer $\text{Cu}(\text{Ac})_2$ and $\text{Zn}(\text{Ac})_2$ particles on the surface of the nanofibers. When the weight ratio was 1:2, these particles could be evenly distributed on the surface of the nanofibers, which provided a seed layer for further hydrothermal growth. When the weight ratio reached 1:1, the nanofibers could no longer accommodate so many particles, resulting in the aggregation of particles and the bundling phenomenon. Therefore, the weight ratio of 1:2 was chosen as the optimum parameter for further study.

FTIR and XRD Analysis

FTIR was used to characterize the CNFMs with different weight ratios ($\text{Cu}(\text{Ac})_2/\text{Zn}(\text{Ac})_2$: PVDF/PAN), and the FTIR spectra of the CNFMs were shown in Fig. 7. It could be seen that the diffraction peaks at 879 cm^{-1} which corresponded to the asymmetric stretching vibration of $-\text{CF}_2-$ in PVDF. The peaks at 1070 cm^{-1} and 1276 cm^{-1} represented the β -phase crystals of PVDF. There was also an obscure peak near 1070 cm^{-1} , which might belong to the stretching vibration of $-\text{C}-\text{C}-$. The peak at 2250 cm^{-1} stood for the stretching vibration of $-\text{CN}-$ in PAN and the peak at 2942 cm^{-1} was the stretching vibration of $-\text{CH}_2-$. The spectra of the CNFMs with $\text{Cu}(\text{Ac})_2$ and $\text{Zn}(\text{Ac})_2$ (b-e) all had a wide diffraction peak at 1573 cm^{-1} , which represented the antisymmetric stretching vibration of $-\text{COO}-$, indicating that $\text{Cu}(\text{Ac})_2$ and $\text{Zn}(\text{Ac})_2$ existed in these CNFMs[38-41]. And the change of the weight ratio ($\text{Cu}(\text{Ac})_2/\text{Zn}(\text{Ac})_2$: PVDF/PAN) had little effects on the spectra.

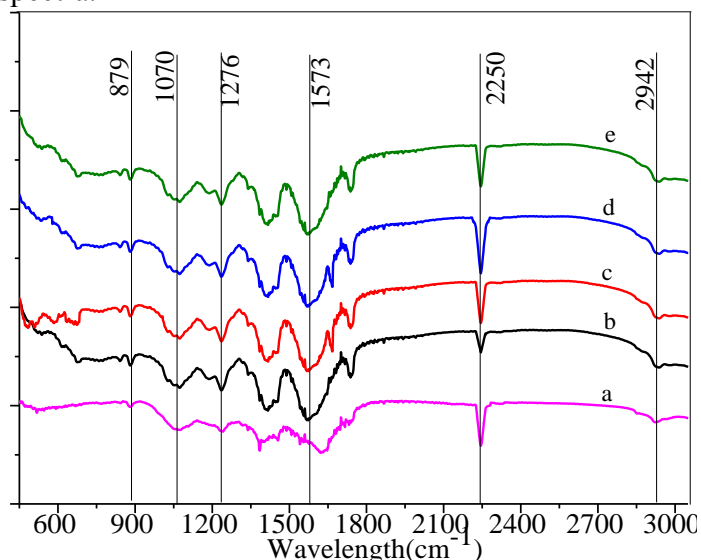


Figure 7. FTIR spectra of the CNFMs with different weight ratios ($\text{Cu}(\text{Ac})_2/\text{Zn}(\text{Ac})_2$: PVDF/PAN) ((a) 0:1 (b) 1:5 (c) 1:3 (d) 1:2 (e) 1:1).

In order to measure the effect of the weight ratio ($\text{Cu}(\text{Ac})_2/\text{Zn}(\text{Ac})_2$: PVDF/PAN) on the crystallization of the CNFMs, XRD analyses were performed and their XRD patterns with distinctive crystalline peaks were shown in Fig. 8 and Fig. 9. Fig. 8 and Fig. 9 displayed that pure $\text{Cu}(\text{Ac})_2$ and $\text{Zn}(\text{Ac})_2$ powders all had obvious diffraction peaks at 7° , and pure PVDF/PAN CNFMs had strong diffraction peaks at 17° and 21° , corresponding to the characteristic peaks of PAN and PVDF respectively. Moreover, the CNFMs with $\text{Cu}(\text{Ac})_2$ and $\text{Zn}(\text{Ac})_2$ (Fig. 8(b-e)) had obvious diffraction peaks at 7° . In addition, as the contents of $\text{Cu}(\text{Ac})_2$ and $\text{Zn}(\text{Ac})_2$ increased the intensity of the peaks corresponding to

$\text{Cu}(\text{Ac})_2$ and $\text{Zn}(\text{Ac})_2$ in XRD spectra of the CNFMs increased, and the diffraction peaks at 34° appeared and increased gradually. At the same time, the diffraction peaks at 21° changed from smooth to sharp gradually, which might be due to the superposition of the diffraction peaks of PVDF with those of $\text{Cu}(\text{Ac})_2$ and $\text{Zn}(\text{Ac})_2$ between 5° and 20° [42-44](Mukhiya et al., 2018, Sethupathy et al., 2014; Miao et al., 2012). The XRD results indicated that there was no new crystalline phase in the CNFMs, and $\text{Cu}(\text{Ac})_2$, $\text{Zn}(\text{Ac})_2$, PVDF and PAN still retained their crystalline structures.

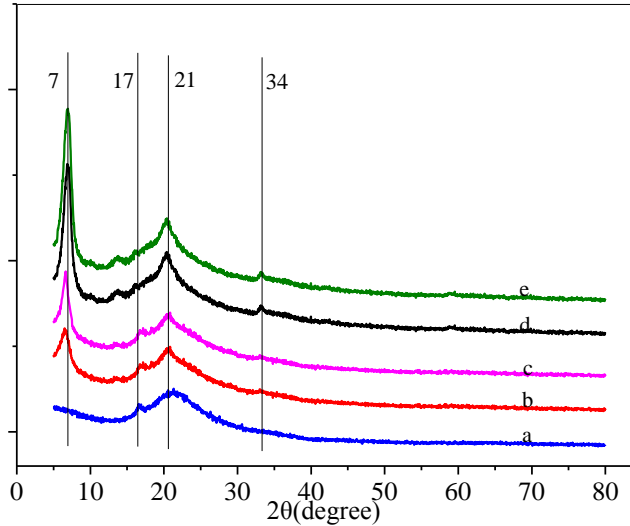


Figure 8. XRD spectra of the CNFMs with different weight ratios ($\text{Cu}(\text{Ac})_2/\text{Zn}(\text{Ac})_2$:PVDF/PAN) ((a) 0:1 (b) 1:5 (c) 1:3 (d) 1:2 (e) 1:1).

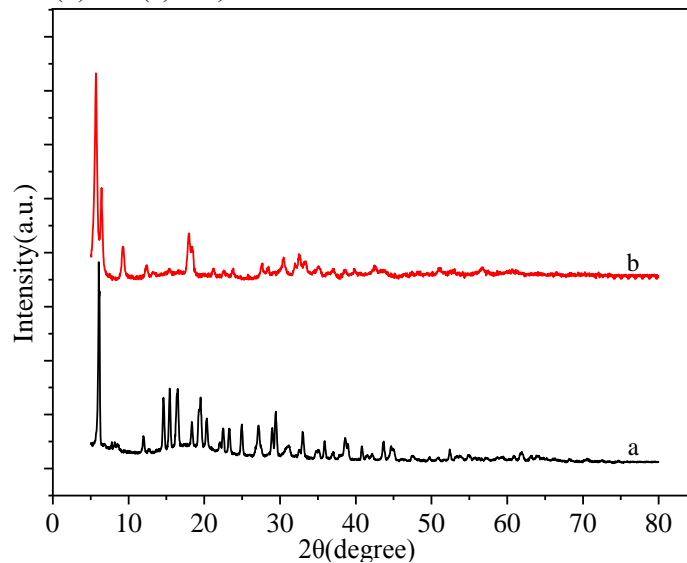


Figure 9. XRD spectra of (a) pure $\text{Cu}(\text{Ac})_2$ powders and (b) pure $\text{Zn}(\text{Ac})_2$ powders.

3.2 Characterization of PVDF/PAN CNFMs with CuO and ZnO nanoparticles

The electrospun PVDF/PAN/ $\text{Cu}(\text{Ac})_2/\text{Zn}(\text{Ac})_2$ CNFMs with the optimum weight ratios ($\text{Cu}(\text{Ac})_2/\text{Zn}(\text{Ac})_2=1:1$, PVDF: PAN=5:5 and $\text{Cu}(\text{Ac})_2/\text{Zn}(\text{Ac})_2$:PVDF/PAN=1:2) were calcined for a period of time, and PVDF/PAN CNFMs with CuO and ZnO nanoparticles were obtained. The effects of heat treatment temperature and time on morphology, structure and properties of the CNFMs were characterized using SEM, FTIR, XRD, and et al.

3.2.1 Effect of the heat treatment temperature on the CNFMs

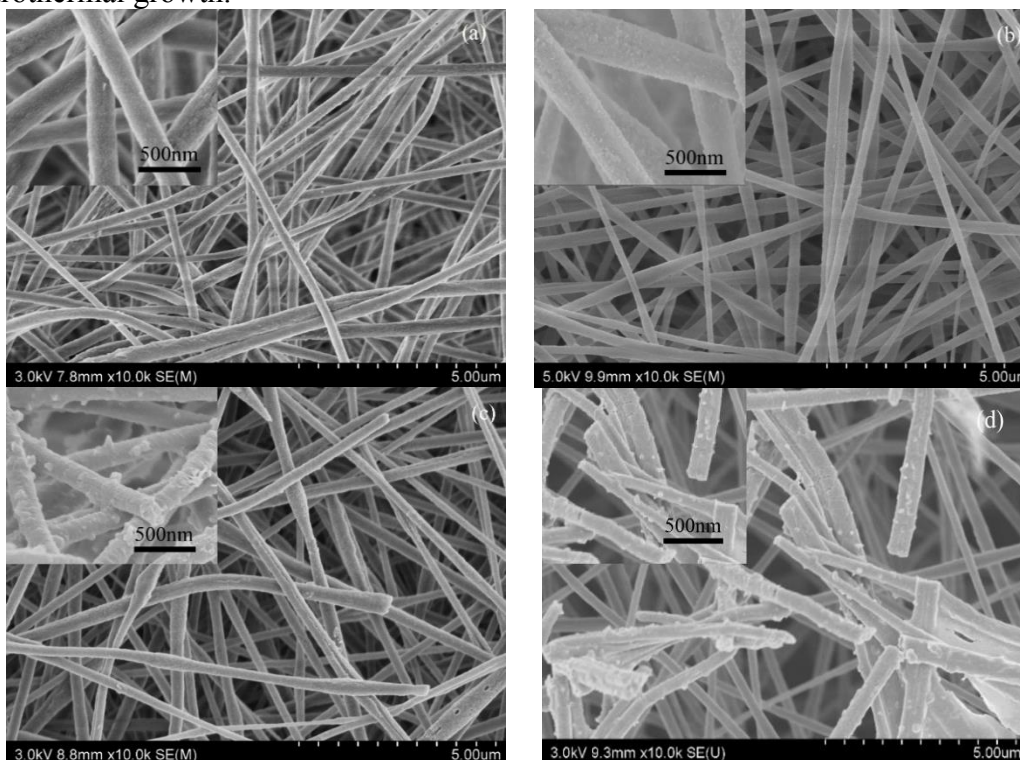
To illustrate the effects of heat treatment temperature on the morphology of the

CNFMs, the temperatures were respectively set to 80°C, 100°C, 120°C, 140°C, 160°C and 180°C, and all the heat treatment times were 2 hours.

Morphological characterization (SEM)

Fig.10 represented the SEM images of PVDF/PAN CNFMs with CuO and ZnO nanoparticles obtained under different heat treatment temperatures for 2 hours. It could be seen that when the temperature was 80°C and 100°C, the morphology of the CNFMs have little change compared with that of the CNFMs without heat treatment, and the surface was still smooth and the whole nanofibers were relatively complete. Then with the increase of the temperature, when the temperature was 120°C, the nanofibers began to break due to the melting of small amounts of PVDF, which was because the melting point of PVDF was generally around 130°C. When the temperature reached 140°C, the nanofibers began to shrink and bend, but they remained fibrous as a whole. When the temperature was 160°C, most of the nanofibers began to melt. Finally, when the temperature was up to 180°C, the PVDF totally melted and the CNFMs no longer had the characteristics of nanofibers.

In addition, as the temperature increased, tiny particles appeared on the surface of the nanofiber, which were CuO and ZnO nanoparticles produced by thermal decomposition of $\text{Cu}(\text{Ac})_2$ and $\text{Zn}(\text{Ac})_2$. Fig.10 (c and d) showed after heat treatment at the temperature of 120-140°C, there were many CuO and ZnO nanoparticles on the surface of nanofibers and they were evenly distributed. When the temperature reached to 160°C, the number and size of nanoparticles on the surface decreased rapidly, as displayed in Fig.10 (e). When the temperature was up to 180°C, the nanoparticles disappeared completely, as indicated in Fig.10 (f). It was because the melted PVDF covered the nanoparticles. Therefore, in the temperature range from 120°C to 140°C, the prepared CNFMs with CuO and ZnO seeds could provide good templates for the subsequent hydrothermal growth.



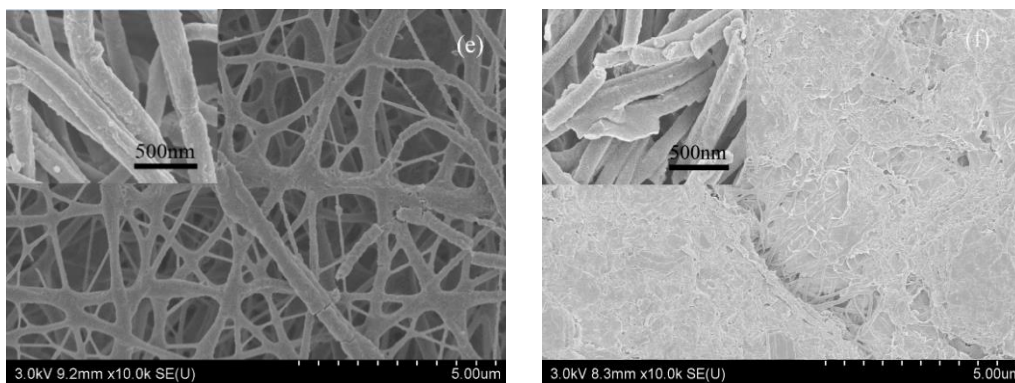


Figure 10. SEM images of PVDF/PAN CNFMs with CuO and ZnO nanoparticles obtained under different heat treatment temperatures for 2 hours ((a) 80°C; (b) 100°C; (c) 120°C; (d) 140°C; (e) 160°C; (f) 180°C).

FTIR and XRD Analysis

In order to further study the effect of heat treatment on the CNFMs, the CNFMs with and without heat treatment were analyzed by FTIR, and the FTIR spectra of the CNFMs were displayed in Fig.11. From the figure we could see that the spectra of the CNFMs with and without heat treatment (Fig.11 (a, b)) as well as PVDF/PAN CNFMs (Fig.11 (c)) all had three diffraction peaks at 1070cm^{-1} , 2250cm^{-1} and 2942cm^{-1} . These three diffraction peaks represented stretching vibration of -C-C- in beta-phase crystals of PVDF, stretching vibration of -CN- in PAN and telescopic vibration of -CH₂- in PAN respectively. By comparison, we concluded that the heat treatment of 140°C had little effects on the PVDF and PAN on the fibrous membranes. The reason might be that the temperature did not reach their melting point. It could also be found that the spectra of the CNFMs with and without heat treatment (Fig.11 (a, b)) as well as Cu(Ac)₂ and Zn(Ac)₂ powders (Fig.11 (d, e)) all had diffraction peaks at 1563cm^{-1} and 1450cm^{-1} , which represented the symmetric and asymmetric vibrations of -COO-. However, the diffraction peaks of the CNFMs with heat treatment for 2 hours at 140°C (Fig.11 (a)) were slightly weakened compared with those of the CNFMs without heat treatment (Fig.11 (b)), which indicated that the chemical reactions of Cu(Ac)₂ and Zn(Ac)₂ occurred during the heat treatment process, and it was likely that CuO and ZnO nanoparticles were formed.

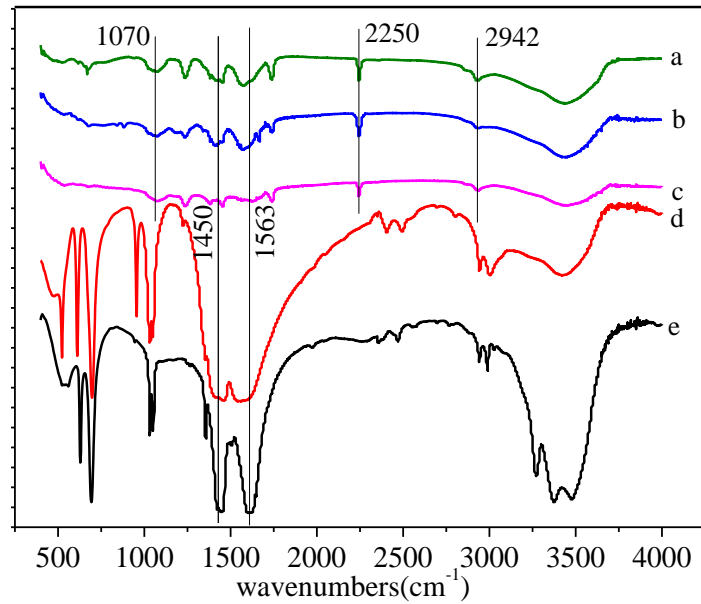


Figure 11. FTIR spectra of (a) the CNFMs with heat treatment for 2 hours at 14°C; (b) the CNFMs without heat treatment; (c) PVDF/PAN CNFMs; (d) Cu(Ac)₂ powders; (e) Zn(Ac)₂ powders.

XRD analyses were performed to the effect of heat treatment on the crystallization of the CNFMs, and their XRD patterns with distinctive crystalline peaks were illustrated in Fig.12. It could be seen that the CNFMs without heat treatment (Fig. 12(b)) had an obvious diffraction peak at 7°, but the CNFMs with heat treatment for 2 hours at 140°C (Fig. 12(a)) showed evident diffraction peaks at 32.6°, 34.8°, 36.5°, 47.5°, 56.5° and 68.2°, corresponding to the characteristic peaks of CuO and ZnO [41]. That meant Cu(Ac)₂ and Zn(Ac)₂ in the CNFMs had been respectively transformed into CuO and ZnO during the heat treatment process, and CuO and ZnO nanoparticles were formed.

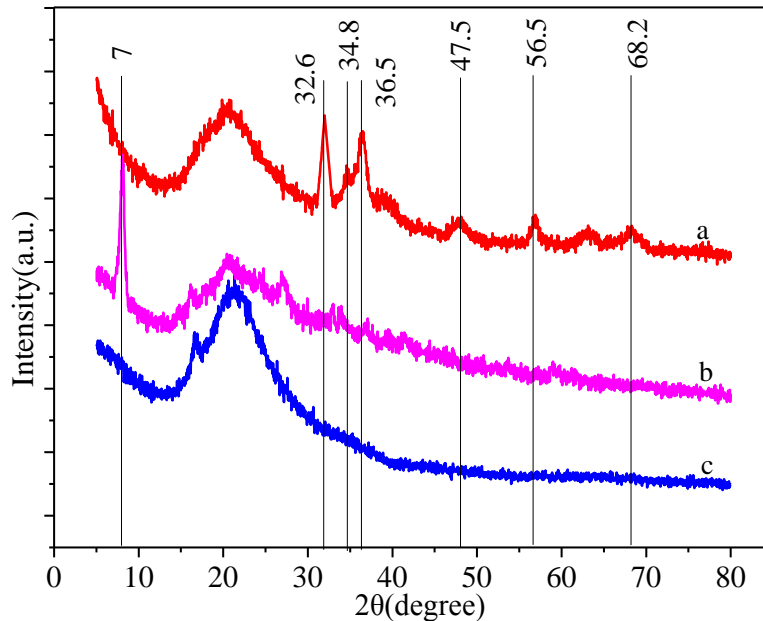


Figure 12. XRD spectra of (a) the CNFMs with heat treatment for 2 hours at 140°C; (b) the CNFMs without heat treatment; (c) PVDF/PAN CNFMs.

Mechanical property

The mechanical properties of PVDF/PAN CNFMs with CuO and ZnO nanoparticles prepared under different heat treatment temperatures for 2 hours were displayed in Fig. 13. It indicated that in the temperature range of 80 to 160°C, the tensile strength of the CNFMs decreased gradually with the increase of the heat treatment temperature, due to the change of nanofiber structure caused by CuO and ZnO nanoparticles produced and the gradual melting of PVDF. At the same time, the carbon chain of PAN molecule vibrated violently and arranged more neatly after the heat treatment, resulting in the decrease of the tensile strength and the brittle fracture of nanofibers under the action of external force. However, when the temperature reached 180°C, the tensile strength of the CNFMs increased suddenly because of the increased adhesion between nanofibers resulting from the almost complete melting of PVDF.

In addition, as the heat treatment temperature increased, the ductility of PVDF became better, resulting in the increase of the breaking elongation of the CNFMs. However, when the temperature rose above 160°C, most of the PVDF began to melt and the soft CNFMs became harder, causing the decrease of the breaking elongation of the CNFMs. Therefore, the CNFMs with better mechanical properties could be prepared by controlling the heat treatment temperature.

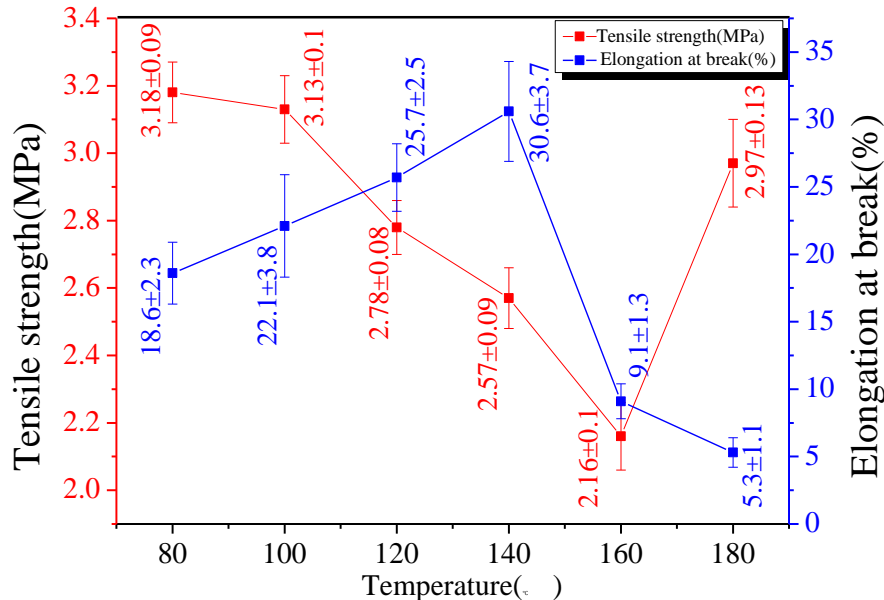


Figure 13. Mechanical properties of the CNFMs obtained under different heat treatment temperatures for 2 hours ((a) 80°C; (b) 100°C; (c) 120°C; (d) 140°C; (e) 160°C; (f) 180°C).

Wetting property

The CA values of the CNFMs without and with the heat treatment obtained were illustrated in Figure 14. It could be seen that the hydrophobicity of the CNFMs with the heat treatment reduced compared with that of the CNFMs without the heat treatment, due to the formation of hydrophilic CuO and ZnO nanoparticles during the heat treatment process. In addition, the hydrophobicity of the CNFMs with the heat treatment gradually decreased with the increase of the heat treatment temperature. It might be that the number of CuO and ZnO nanoparticles produced increased as the temperature increased, but with the further increase of the temperature, the decrease of the hydrophobicity of the CNFMs became smaller and smaller, indicating that Cu(Ac)₂ and Zn(Ac)₂ in the CNFMs had been almost completely transformed into CuO and ZnO under the higher heat treatment

temperature.

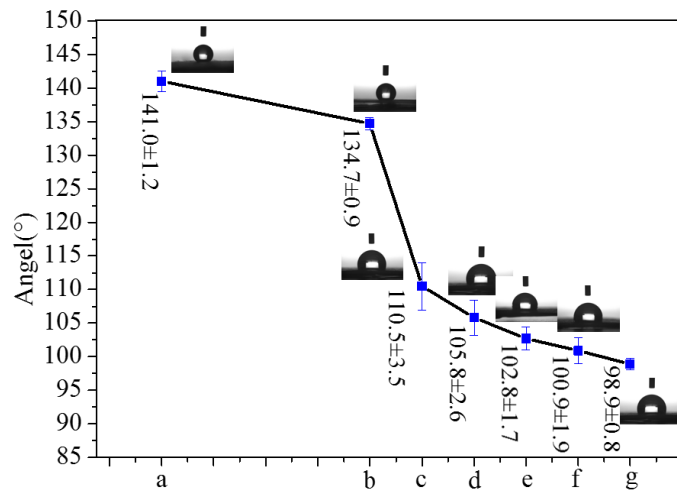


Figure 14. Contact angles of (a) the CNFMs without heat treatment and (b-g) the CNFMs with heat treatment for 2 hours ((b) 80°C; (c) 100°C; (d) 120°C; (e) 140°C; (f) 160°C; (g) 180°C).

3.2.2 Effect of the heat treatment time on morphology of the CNFMs

Fig.15 displayed the SEM images of PVDF/PAN CNFMs with CuO and ZnO nanoparticles obtained undergone heating for different times at 130°C, and the times were set to 2h, 6h and 18h respectively. It illustrated that the longer the heat treatment time was, the more CuO and ZnO nanoparticles were produced. Therefore, the heat treatment time of 18h was selected as the subsequent experimental parameter.

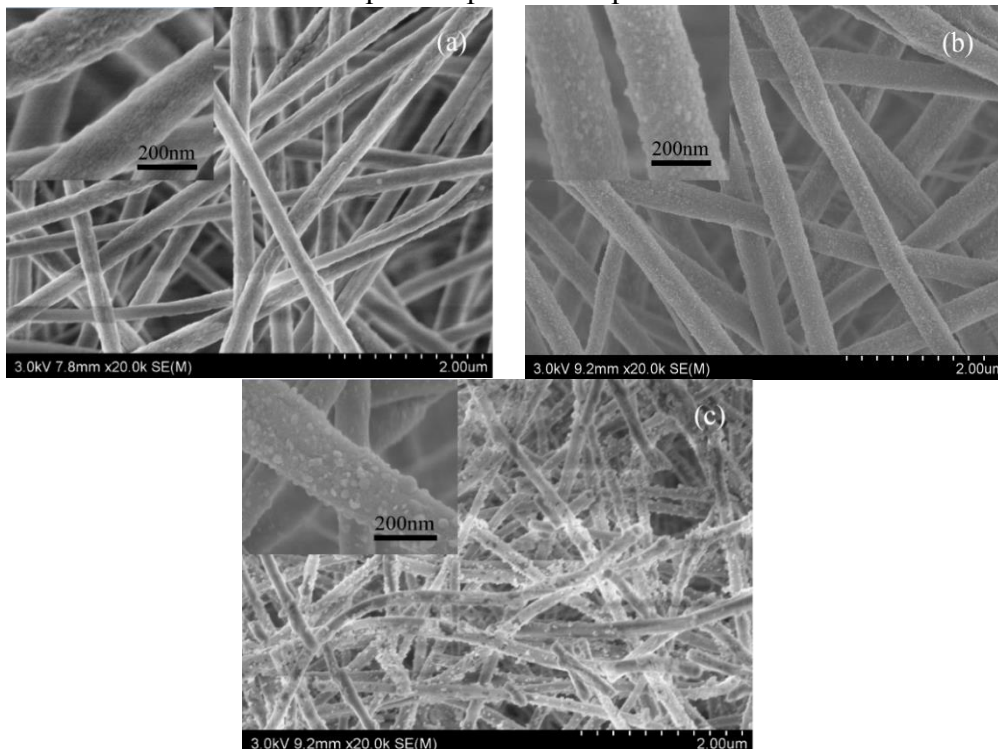


Figure 15. SEM images of PVDF/PAN CNFMs with CuO and ZnO nanoparticles obtained undergone heating for different times at 130°C ((a) 2h; (b) 8h; (c) 16h).

3.3 Characterization of hetero-structured CuO-ZnO loaded CNFMs

Based on the above PVDF/PAN CNFMs with CuO and ZnO nanoparticles obtained by the heat treatment of 18 hours at 140°C, the hetero-structured CuO-ZnO loaded CNFMs were fabricated by hydrothermal method. Then the effects of growth solution

concentration, hydrothermal temperature and hydrothermal time on the morphology of the hetero-structured CuO-ZnO loaded CNFMs were investigated by SEM. And the structure and wetting property of the CNFMs were studied using XRD, EDS and et al.

3.3.1 Effect of the growth solution concentration on morphology of the CNFMs

The sizes and structure of CuO and ZnO nanocrystals varied gradually with the increase of the growth solution concentration under the hydrothermal condition at 120°C for 12 hours, as shown in Fig. 16. It represented with the decrease of the diluted times the growth solution concentration increased, and the high growth solution concentration was more conducive to the formation of hetero-structured CuO-ZnO. When the dilution multiple was 25 times, CuO and ZnO crystals with irregular shapes and sizes were deposited on the surface of nanofibers and piled up in disorder. When the dilution multiple was 5 times, CuO and ZnO crystals were stacked on the surface of nanofibers in the granule-like and sheet-like structure, and their distributions were not uniform. When the dilution multiple was 1 time, the whole nanofiber surface was encapsulated by CuO and ZnO crystals, forming a heterostructure similar to honeycomb. When the growth solution was saturated, CuO and ZnO crystals with regular polygonal sheet-like structure, similar to petals, were uniformly distributed on the whole nanofiber surface, leading to a very large specific surface area. Therefore, the saturated growth solution would be used in the subsequent experiments.

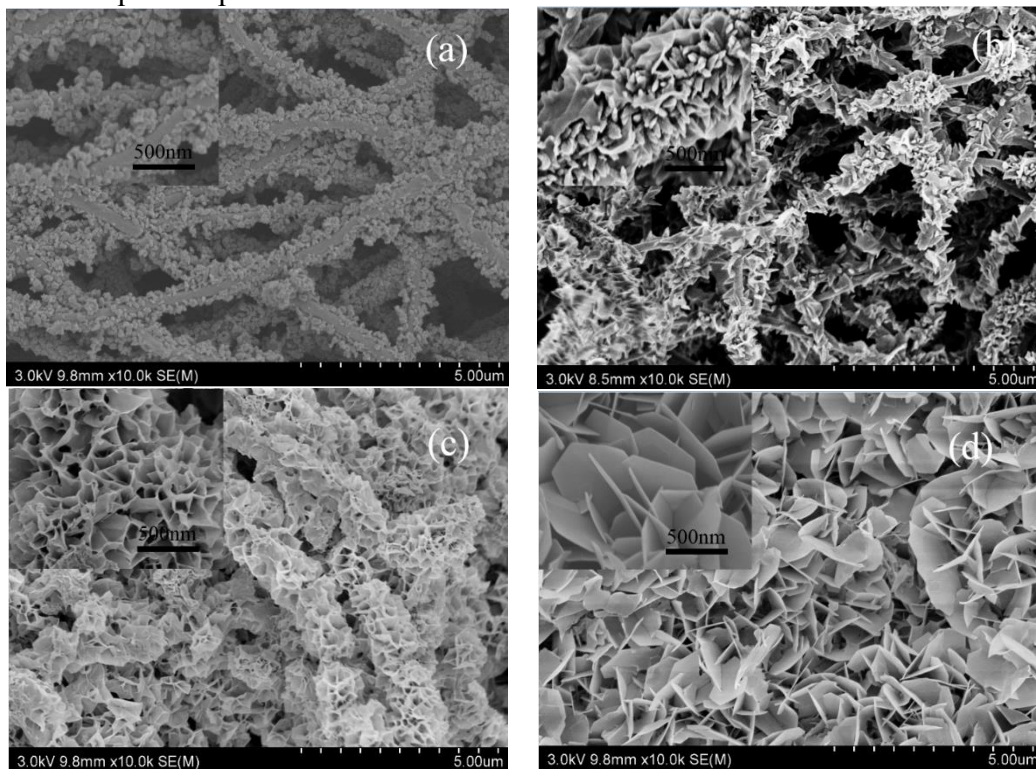


Figure.16 SEM images of hetero-structure CuO-ZnO loaded CNFMs obtained using different growth fluid concentrations under the hydrothermal condition ((a) 25 times dilution (b) 5 times dilution (c) 1 time dilution (d) saturated solution).

3.3.2 Effect of the hydrothermal temperature on morphology of the CNFMs

Figure 17 displayed the SEM images of hetero-structure CuO-ZnO loaded CNFMs prepared using the saturated growth solution at different hydrothermal temperatures for 12 hours, respectively. It could be seen that when the hydrothermal temperature was 80°C, the surface of nanofibers was covered by a layer of thick pebble-like nanoparticles. When the hydrothermal temperature was 100°C, the CuO-ZnO heterostructure obtained was

similar to honeycomb. When the hydrothermal temperatures were 120°C, 140°C and 160°C, the CuO-ZnO heterostructures formed were petal-like and resembled flowers. However, the heterostructures obtained at 120°C and 140°C were much more regular and thinner than those obtained at 160°C. When the temperature reached 180°C, the nanofibers began to shrink due to the melting of PVDF, and the CuO-ZnO heterostructure couldn't be formed. Therefore, the hydrothermal temperature would be 120°C-140°C in the subsequent experiments.

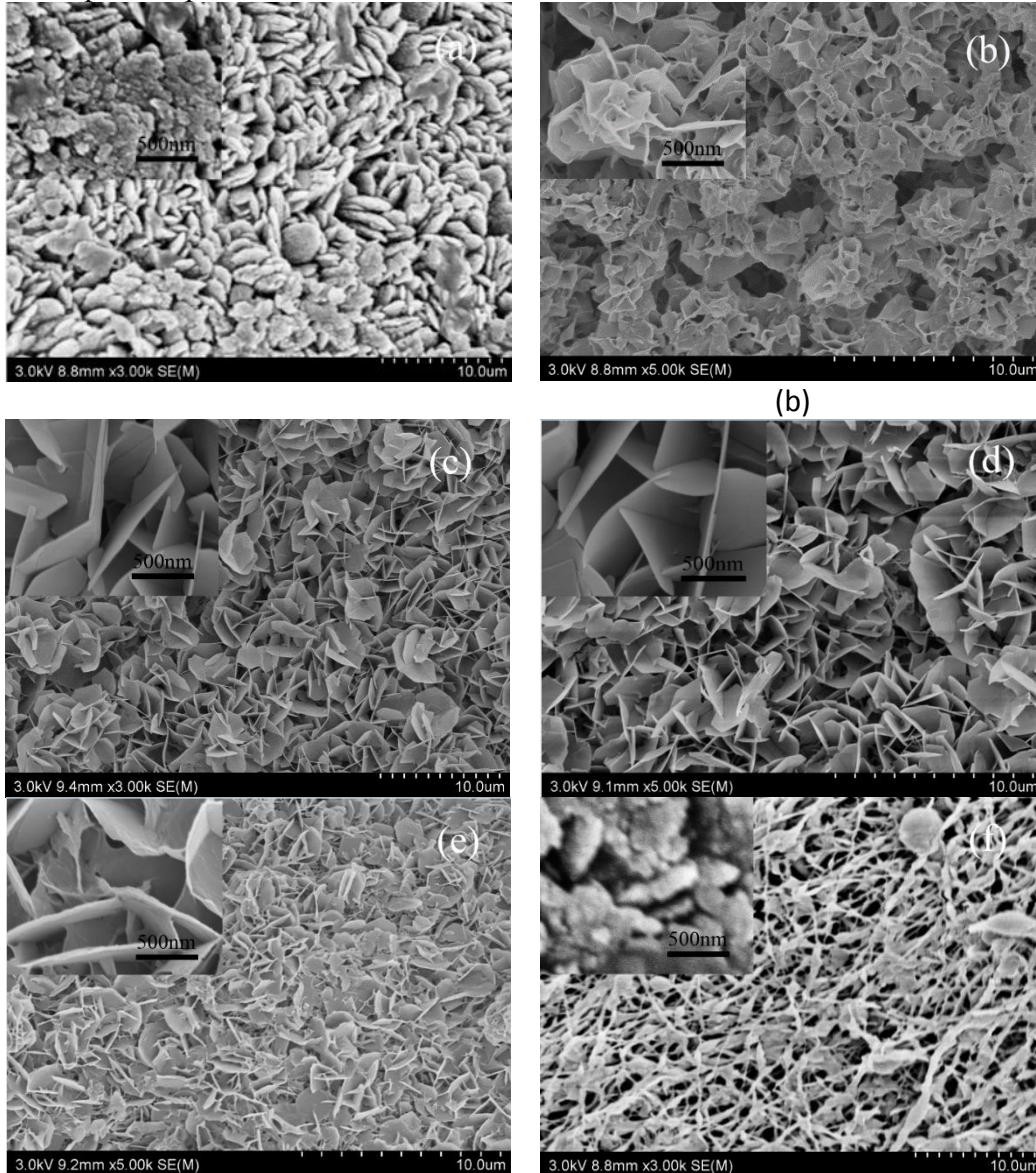


Figure 17. SEM images of hetero-structure CuO-ZnO loaded CNFMs with different hydrothermal temperatures ((a) 80°C; (b) 100°C; (c) 120°C; (d) 140°C; (e) 160°C; (f) 180°C).

3.3.3 Effect of the hydrothermal time on morphology of the CNFMs

The hetero-structured CuO-ZnO loaded CNFMs were fabricated using the saturated growth solution under the hydrothermal condition at 120°C for different hydrothermal times, and their SEM images were exhibited in Fig.18. Fig.18 showed that when the hydrothermal time was 6 hours, the CuO-ZnO heterostructures were petal-like sheets with distinct edges and corners, and the stacking was regular. When the hydrothermal time was 12 hours, the CuO-ZnO heterostructures were also petal-like sheets, but they were thicker

than those of the hydrothermal time of 6 hours. When the hydrothermal time was 18 hours, the whole CuO-ZnO heterostructure was similar to a honeycomb due to the continuous stacking of the sheets. And with the increase of the hydrothermal time, more and more sheets were constantly formed and stacked. When the hydrothermal time was up to 24 hours, the CuO-ZnO heterostructures became disorderly. This was because that too many sheets were produced and accumulated. Therefore, the selected hydrothermal time in the subsequent experiments would be 6 hours.

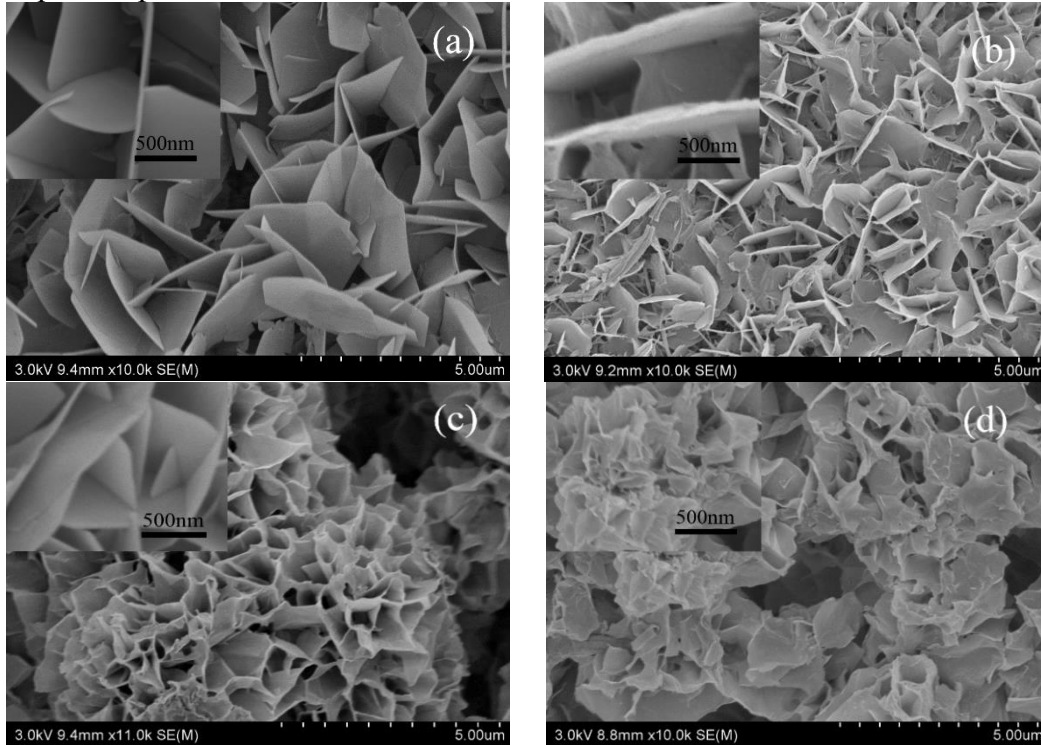


Figure 18. SEM images of hetero-structured CuO-ZnO loaded CNFMs under different hydrothermal times ((a) 6h; (b) 12h; (c) 18h; (d) 24h).

3.3.4 XRD and EDS Analysis of the CNFMs

X-ray diffraction spectrum of hetero-structured CuO-ZnO loaded CNFMs was illustrated in Fig.19. It could be seen that the crystallization peaks of PAN and PVDF were at 17° and 21° respectively, and the superposition peak of $\text{Cu}(\text{Ac})_2$ and $\text{Zn}(\text{Ac})_2$ was at 7° , indicating the existence of $\text{Cu}(\text{Ac})_2$ and $\text{Zn}(\text{Ac})_2$ due to their incomplete decomposition during heat treatment. In addition, there was a strong diffraction peak at about 35.7° formed by CuO and ZnO together. The diffraction peaks at 44.5° and 66.4° belonged to ZnO, while those at 40.3° , 58.5° , 53.5° and 61.3° belonged to CuO. However, these peaks were slightly offset due to the interaction of CuO and ZnO[45-47]. XRD patterns showed that CuO-ZnO heterostructures had been formed on the surface of the nanofibers.

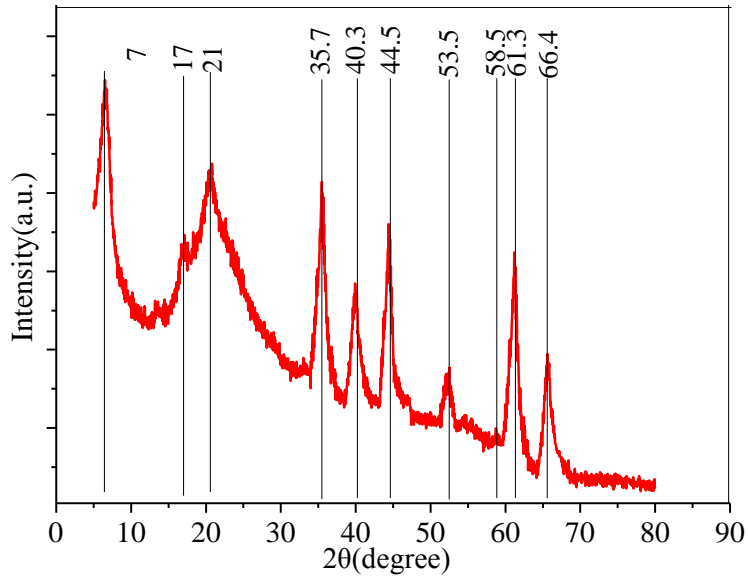
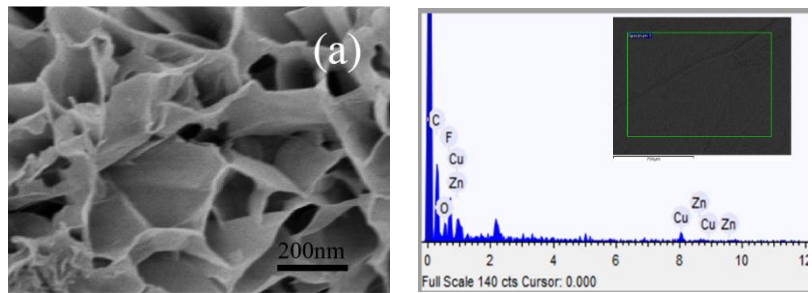
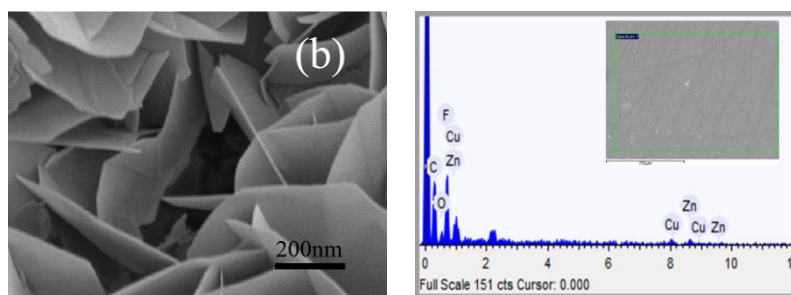


Fig.19 X-ray diffraction spectrum of hetero-structured CuO-ZnO loaded CNFMs

Fig. 20 showed the EDS spectra of two hetero-structured CuO-ZnO loaded CNFMs with different macroscopic colors and microstructures, and it could be found that the difference between them was due to the different contents of Cu and Zn in the CNFMs. The proportion of Cu and Zn in Fig.20 (a) was larger than that in Fig.20 (b) due to more formed and stacked CuO-ZnO sheets, resulting in the darker color of CNFMs. In addition, in Fig.20 (a), the proportion of Cu and Zn was 3:2, which might be caused by the faster growth of CuO crystals than that of ZnO crystals. But in Fig.20 (b), the proportion of Cu and Zn was 1:1, which indicated that the growth rates of CuO and ZnO crystals were close to each other, and the CuO-ZnO heterostructures formed were petal-like sheets with distinct edges and corners.



Element	Weight %	Atomic %
C	26.623	20.326
H	5.937	54.383
O	10.829	6.201
N	11.220	7.337
F	15.674	7.557
Cu	17.908	2.501
Zn	11.809	1.695

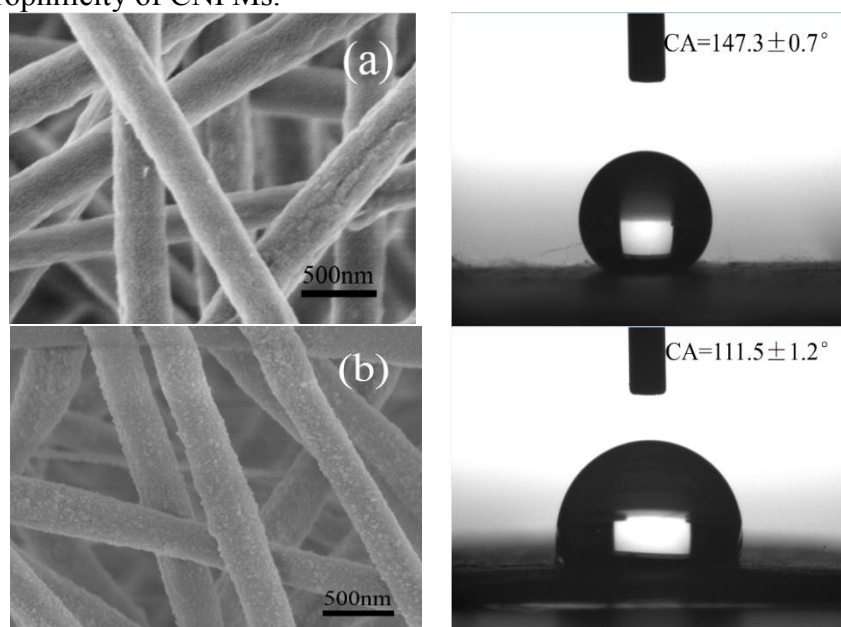


Element	Weight %	Atomic %
C	35.110	23.515
H	6.598	53.026
O	4.561	2.290
N	15.874	9.114
F	24.630	10.415
Cu	7.207	0.884
Zn	6.020	0.756

Figure 20. Element compositions of CNFMs with different CuO-ZnO heterostructures.

3.3.5 Wetting property of the CNFMs

The effect of CuO-ZnO heterostructure on the wettability of CNFMs was investigated, and the morphologies and CA of CNFMs before and after heat treatment and hydrothermal growth were indicated in Fig. 21. The results showed the wettability of the CNFMs changed from hydrophobicity to hydrophilicity after heat treatment and hydrothermal growth. The main reason was that hydrophilic CuO and ZnO grew on the surface of nanofibers, and the hydrophilic mechanism was illustrated in Fig.22. It could be seen that when hydrophilic CuO and ZnO were loaded on the surface of nanofibers, water droplets would be immersed in the gaps of the CuO-ZnO flaky structures, leading to the hydrophilicity of CNFMs.



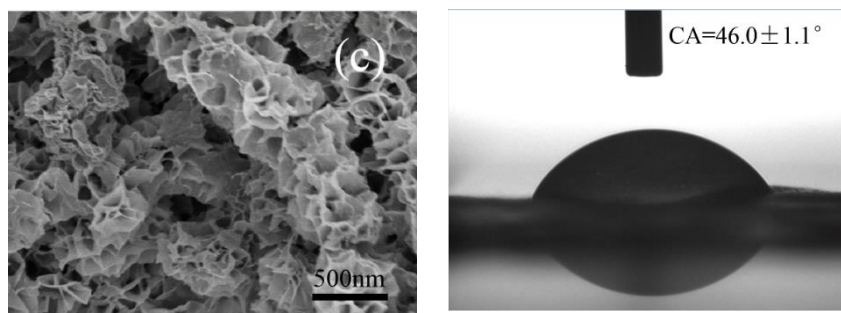


Figure 21. Morphologies and CA of the CNFMs before and after heat treatment and hydrothermal growth ((a) without heat treatment; (b) with heat treatment; (c) with heat treatment and hydrothermal growth)

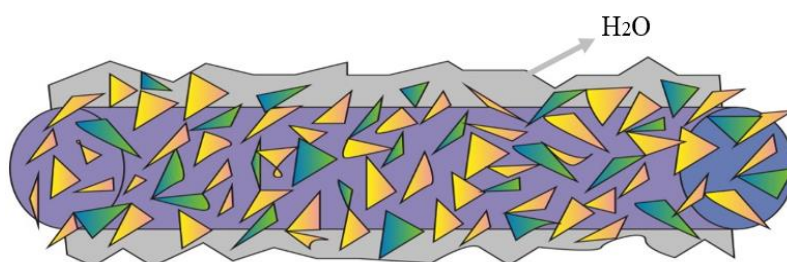


Figure 22. Hydrophilic Mechanism of CNFMs with CuO-ZnO heterostructures

3.4 Photocatalytic degradation experiment

The experiments of photocatalytic degradation under UV irradiation were carried out using the four prepared CNFMs degrading methyl orange solution with the concentration of 10mg/L. The four kinds of CNFMs were electrospun PVDF/PAN CNFMs, CuO loaded PVDF/PAN CNFMs, ZnO loaded PVDF/PAN CNFMs and hetero-structured CuO-ZnO loaded PVDF/PAN CNFMs, named A, B, C and D, respectively. The absorbance measured by UV spectrophotometer, corresponding to the solution at each time interval in the degradation process, were shown in Table 4. And the degradation rate of methyl orange, defined as η , was calculated by the following formula, as illustrated in Table 4 and Fig.23.

$$\eta = \frac{\text{Absorbance of the original solution} - \text{Absorbance of the current solution}}{\text{Absorbance of the original solution}} \times 100\%$$

Table 4. Absorbance and degradation rate of methyl orange solutions at different time intervals using A, B, C and D samples.

Time (hour)	0	1	2	3	4	5	24	
Absorbance	A	0.396	0.390	0.390	0.390	0.384	0.370	0.366
	B	0.396	0.374	0.229	0.169	0.107	0.056	0.048
	C	0.396	0.342	0.20	0.175	0.104	0.052	0.037
	D	0.396	0.334	0.279	0.154	0.086	0.032	0.029
Degradation rate (%)	A	0	1.5	1.5	1.5	3.1	6.7	7.6
	B	0	5.6	42.2	57.3	73.7	85.9	87.9
	C	0	13.6	49.5	55.8	73.7	86.9	90.7
	D	0	15.7	29.5	43.1	67.6	92.2	92.7

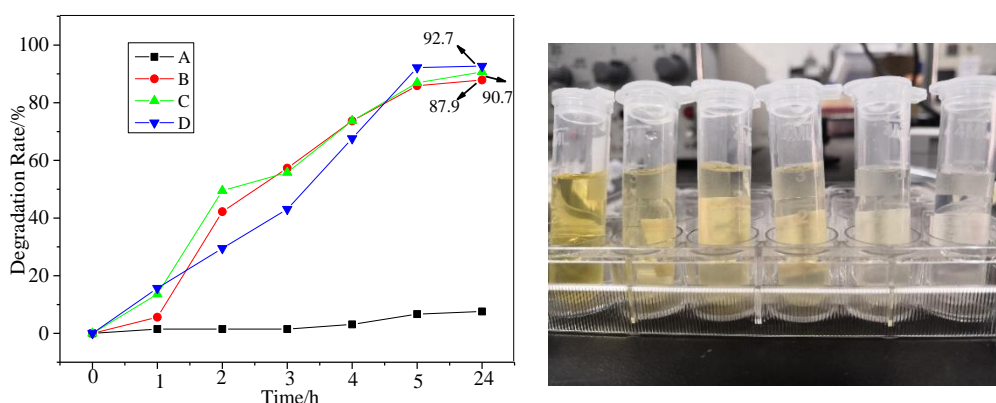


Figure 23. The diagram of degradation rate of methyl orange solutions at different time intervals using A, B, C and D samples. The right figure was the photo of degradation of methyl orange solutions at different time intervals using the D sample.

It could be seen that the sample A had almost no photocatalytic degradation of methyl orange, and the final degradation rate of 6.7% was likely due to the adsorption of a small amount of methyl orange on the CNFMs. The samples B, C and D all had a good photocatalytic degradation effect on methyl orange. Especially, the photocatalytic degradation rate of the sample D almost reached the maximum after 5 hours. Compared with the final degradation rate of sample B and sample C, that of sample D was highest and up to 92.7%. That meant the hetero-structured CuO-ZnO loaded CNFMs had the best photocatalytic degradation effect of methyl orange due to the broader UV adsorption region of the hetero-structured CuO-ZnO than that of CuO and that of ZnO.

The mechanism of photocatalytic degradation of methyl orange using the hetero-structured CuO-ZnO loaded CNFMs was illustrated in Fig. 24. It could be seen that when the UV light irradiated the hetero-structured CuO-ZnO on the CNFMs, the valence band (VB) electrons gained energy and passed through the band gap to the conduction band (CB), resulting in the formation of electron-hole pairs. The photoexcited holes of VB showed strong oxidizability and the CB electrons exhibited reducibility, leading to the photocatalytic degradation of methyl orange. In addition, a large number of p-n heterojunctions composed of ZnO and CuO were formed due to the combination of *p*-type CuO and *n*-type ZnO. Under UV irradiation, the excited electrons on the CB of CuO could easily transfer to the CB of ZnO, whereas the holes in the VB of ZnO could migrate into the VB of CuO. Therefore, the numbers of photoexcited holes on the hetero-structured CuO-ZnO increased [48], which would lead to the higher photocatalytic activity of the hetero-structured CuO-ZnO.

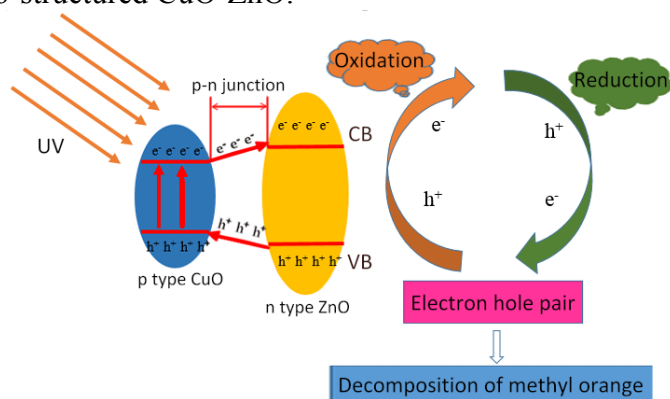


Figure 24. The mechanism schematic of photocatalytic degradation of methyl orange using the hetero-structured CuO-ZnO loaded CNFMs.

After consecutive photocatalytic degradation of three 10 mg/L methyl orange solution with 30 mL for 5 hours using the same sample D, the final degradation rate data were illustrated in Table 5. It showed the degradation rates of the hetero-structured CuO-ZnO loaded CNFMs decreased after repeated photocatalytic degradation experiments for three times, but the degradation rate decreased slightly, and still maintained more than 90%. That meant the hetero-structured CuO-ZnO loaded CNFMs could be reused to degrade methyl orange at least three times.

Table 5. The degradation rates after consecutive photocatalytic degradation using the sample D.

Number of times	Absorbance		Degradation rate (%)
	0h	5h	
1	0.396	0.029	92.2
2	0.396	0.033	91.4
3	0.396	0.039	90.1

4. Conclusions

In this paper, the hetero-structured CuO-ZnO loaded CNFMs were prepared by a combination of electrospinning technology, heat treatment and hydrothermal method. The effects of electrospinning, heat treatment and hydrothermal parameters on morphology, structure and properties of the CNFMs were investigated, and the optimal process parameters were determined. The results showed that when $\text{Cu}(\text{Ac})_2 : \text{Zn}(\text{Ac})_2 = 1:1$, PVDF: PAN=5:5 and $\text{Cu}(\text{Ac})_2/\text{Zn}(\text{Ac})_2:\text{PVDF}/\text{PAN}=1:2$, the morphology and mechanical property of the electrospun CNFMs were relatively better and the $\text{Cu}(\text{Ac})_2$ and $\text{Zn}(\text{Ac})_2$ nanoparticles were evenly distributed on the surface of the nanofibers. When the heat treatment temperature was in the range of 120°C-140°C and the duration of heat treatment was 18h, the morphology, structure and mechanical properties of CuO and ZnO loaded CNFMs were relatively better. When the growth solution was saturated, the hydrothermal temperature was 120°C-140°C and the hydrothermal synthesis hours was 6h, the morphology and structure of hetero-structured CuO-ZnO on the CNFMs were the best.

Then the hetero-structured CuO-ZnO loaded CNFMs prepared under the condition of the optimal process parameters were applied to photocatalytic degradation of methyl orange, and its mechanism of photocatalytic degradation was investigated. The photocatalytic degradation of methyl orange was carried out for 24 h, and the final degradation rate was 92.7%, which was higher than CNFMs with CuO or ZnO only. In addition, the hetero-structured CuO-ZnO loaded CNFMs could be reused to degrade methyl orange at least three times, and the degradation rate remained above 90%.

Author Contributions

Lan Xu and Liang Yu designed the experiments; Liang Yu and Wei Fang performed the experiments; Liang Yu and Wei Fang did the characterization; Lan Xu and Liang Yu analyzed the data; Wei Fang, Liang Yu and Lan Xu wrote the paper; Lan Xu revised the paper.

Acknowledgments

The work is supported financially by National Natural Science Foundation of China (Grant No. 11672198), Six Talent Peaks Project of Jiangsu Province (Grant No. GDZB-050), Foundation project of Jiangsu Advanced Textile Engineering Technology Center (Grant No. XJFZ/2018/15), and PAPD (A Project Funded by the Priority Academic Program Development of Jiangsu Higher Education Institutions).

References

1. Bachmann J, Hidalgo C, Stéphanie B. *Science China Technological Sciences* 60 (2017) 1301-1317.
2. Qureshi N, Shinde M, Arbuñ S. *Journal of Nanoscience and Nanotechnology* 54 (2019) 479-486.
3. Meng XF, Han QX, Tang Q. *Journal of Nanoscience and Nanotechnology* 19 (2018) 786-794.
4. Li F, Wang GY, Zhang Y. *Journal of Chemistry of Colleges and Universities* 36 (2015) 1351-1357.
5. E. Pelizzetti, N. Serpone (Eds.). *Photocatalysis*, Wiley, New York 58 (1989) 46-52.
6. A. Di Paola, M. Addamo; V. Augugliaro. *Catalysis Today* 58 (2000) 141-149.
7. Jayasekharan T. *Chemical Physics Letters* 699 (2018) 48-54.
8. Kim JH, Mirzaei A, Zheng YL. *Sensors & Actuators: B-Chemical* 281 (2019) 543-562.
9. Ma YX, Shao WJ, Sun W. *Applied Surface Science* 459 (2018) 544-553.
10. Waldner G, Pourmodjib M, Bauer R. *Chemosphere* 50 (2003) 989-998.
11. Lucas-Gil ED, Campo AD, Pascual L. *Materials Science & Engineering C-Materials for Biological Applications* 99 (2019) 575-581.
12. Wang H, Gong XC, Miao YL. *Food Chemistry* 283 (2019) 397-403.
13. Pan TD, Li ZJ, Shou DH, Shou W, Fan JT, Liu X, Liu Y. *Advanced Materials Interfaces*, 2019, 1901130.
14. Chakraborty P, Dhar S, Debnath D. *Sensors & Actuators: B. Chemical* 283 (2019) 776-785.
15. Zhang T, Tang X, Zhang J. *Langmuir* 34 (2018) 14577-14585.
16. Liu C, Meng F, Zhang L. *Applied Surface Science* 465 (2018) 276-282.
17. Heng CL, Xiang W, Su WY. *Journal of Luminescence* 210 (2019) 363-370.
18. Liu LQ, Cao GX, Hong KG. *Journal of Wuhan University of Technology (Materials Science)* 33 (2018) 1372-1375.
19. Al-Hadeethi Y, Umar A, Singh K. *Journal of Nanoscience and Nanotechnology* 19 (2019) 4199-4204.
20. Lei Q, Li H, Zhang H. *Journal of Semiconductors* 40 (2019) 17-23.
21. Wu X, Xu J, George Y. *Green Energy & Environment* 2 (2017) 387-392.
22. Chakraborty P, Dhar S, Debnath K. *Sensors & Actuators: B. Chemical* 283 (2019) 776-785.
23. Liu ZL, Deng JC, Deng JJ. *Materials Science and Engineering: B* 150 (2008) 99-104.
24. Wei SQ, Chen YY, Ma YY. *Journal of Molecular Catalysis A: Chemical* 331 (2010) 112-116.
25. Fierro G, Jacono M L O, Invers MI. *Applied Catalysis A: General* 137 (1996) 327-348.
26. Atta A, Al-Lohedan H, Ezzat A. *Journal of Molecular Liquids* 236 (2017) 38-47.
27. Zha Jinlong, Batisse Nicolas, Claves Daniel, Dubois Marc. *Journal of colloid and in*

- terface science 6 (2019) 778-787.
28. Qavamnia SS, Nasouri K. *Fibers and Polymers* 17 (2016) 1977-1984.
 29. Shao ZB, Xu L, Wang MD. *Nanoscale Research Letters* 12 (2017) 470.
 30. Yasemin DI, Ilyas D, Bedrettin M. *International Journal of Biological Macromolecules* 96 (2016) 302-311.
 31. Fang Y, Xu L. *Beilstein Journal of Nanotechnology* 2261-2274.
 32. Song YH, Sun ZY, Xu L, Shao ZB. *Polymers* 9 (2017) 12-17.
 33. Wang FF, Sun ZY, Yin J, Xu L. *Nanomaterials* 9 (2019) 508.
 34. He Y, Liu Y. *Journal of Central South University* 25 (2018) 2182-2189.
 35. Yuan Y, Zhang JY, Fan GX, Zhao YC, Zheng CG. *Chinese Journal of Electrical Engineering* 32 (2012) 44-49.
 36. Teng LT, Zhao K, Wang HZ, Tang YF. *Journal of Molecular Liquids* 43 (2014) 3175-3179.
 37. Malwal, D, Gopinath, P. *Efficient. Journal of Hazardous Materials* 321 (2017) 611-621.
 38. Karwoth T, Zeng XL, Koblischka MR. *Solid State Communications* 290 (2019) 37-41.
 39. Kumar MS, Madhumita B, Arun M. *Journal of Colloid and Interface Science* 51 (2018) 592-601.
 40. Khenfouch M, Baïtoul M, Maaza M. *Raman. Optical Materials* 36 (2013) 27-37.
 41. Mazhdi M, Tafreshi MJ. *Applied Physics A-materials Science & Processing* 124 (2018) 564-572.
 42. Mukhiya K, Lubasova D, Qureshi N. *Sensors and Actuators B: Chemical* 275 (2018) 322-331.
 43. Sethupathy M, Pandey P, Manisankar P. *Journal of Applied Polymer Science* 131 (2014) 58-71.
 44. Miao L, Zhang H, Zhu Y. *Journal of Materials Science: Materials in Electronic* 23 (2012) 1887-1890.
 45. Ye Q, Chen XH, Yang J, Wu DT. *Food chemistry* 287 (2019) 375-381.
 46. Chol SW, Katoch A, Zhang J. *Sensors and Actuators B-Chemical* 176 (2013) 585-591.
 47. Li Y, Jiao M, Yang M. *Sensors and Actuators B: chemical* 238 (2017) 596-604.
 48. Xu HY, Shi ML, Liang CQ. *Nanoscale Research Letters* 13 (2018) 195.